



**AIAA-2001-0759**

**Development of a Semi-Span Test Capability at  
the National Transonic Facility (Invited)**

G. M. Gatlin, P. A. Parker, and L. R. Owens, Jr.  
NASA Langley Research Center  
Hampton, Virginia

**39th AIAA Aerospace Sciences Meeting & Exhibit**  
8-11 January 2001  
Reno, Nevada



## DEVELOPMENT OF A SEMI-SPAN TEST CAPABILITY AT THE NATIONAL TRANSONIC FACILITY (INVITED)

G. M. Gatlin,\* P. A. Parker,† and L. R. Owens, Jr.\*  
 NASA Langley Research Center  
 Hampton, VA 23681-2199

### Abstract

A need for low-speed, high Reynolds number test capabilities has been identified for the design and development of advanced subsonic transport high-lift systems. In support of this need, multiple investigations have been conducted in the National Transonic Facility (NTF) at the NASA Langley Research Center to develop a semi-span testing capability that will provide the low-speed, flight Reynolds number data currently unattainable using conventional sting-mounted, full-span models. Although a semi-span testing capability will effectively double the Reynolds number capability over full-span models, it does come at the expense of contending with the issue of the interaction of the flow over the model with the wind-tunnel wall boundary layer. To address this issue the size and shape of the semi-span model mounting geometry have been investigated, and the results are presented herein. The cryogenic operating environment of the NTF produced another semi-span test technique issue in that varying thermal gradients have developed on the large semi-span balance. The suspected cause of these thermal gradients and methods to eliminate them are presented. Data are also presented that demonstrate the successful elimination of these varying thermal gradients during cryogenic operations.

### Introduction

The development of a semi-span model test capability has been proposed for the National Transonic

Facility (NTF) at the NASA Langley Research Center. This capability is required for the development of advanced high-lift systems for future, large subsonic transport aircraft at near flight Reynolds numbers. The semi-span testing technique has been suggested as a tool that should be developed to provide state-of-the-art wind tunnel research capabilities.<sup>1,2</sup> The current full-span model test capability at the NTF cannot produce results at flight Reynolds numbers for large subsonic transport aircraft at takeoff and approach conditions. Due to the sensitivity of high lift configurations to Reynolds number,<sup>1</sup> performance characteristics obtained at Reynolds numbers below flight conditions may result in non-optimized high-lift systems.

Semi-span model testing can provide an increased Reynolds number capability simply due to increased model size. In general, the Reynolds number capability can be doubled when a semi-span model is used in place of a full-span model. An illustration of low-speed, high Reynolds number test capabilities, and the increased Reynolds number capability provided by semi-span testing at the NTF, is presented in figure 1. Several large subsonic transport aircraft, at the representative approach speed of  $M_\infty = 0.2$ , are noted. Information presented in figure 1 illustrates the need for a semi-span test capability at the NTF in order to achieve flight Reynolds number for large transport aircraft at takeoff and approach conditions. Additional benefits of semi-span testing include improved model fidelity, reduced aeroelastic effects, and reduced model costs. However, these benefits are offered at the expense of the interaction of the flow over the semi-span model with the wind-tunnel wall boundary layer, as well as wall interference effects due to increased model size.

To further understand the flow physics involved in semi-span testing as well as to develop techniques to minimize the effects of the wall boundary layer, both experimental and computational studies have been utilized.<sup>3,4</sup> It is recognized that minimizing or

\*Research Scientist, Subsonic Aerodynamics Branch, Senior Member AIAA

†Research Scientist, Model Systems Branch, Member AIAA

Copyright © 2001 by the American Institute of Aeronautics and Astronautics, Inc. No copyright is asserted in the United States under Title 17, U.S. Code. The U.S. Government has a royalty-free license to exercise all rights under the copyright claimed herein for Governmental purposes. All other rights are reserved by the copyright owner.

eliminating the wall boundary layer will certainly improve the effectiveness of a semi-span test capability;<sup>5</sup> however, the implementation of an active sidewall boundary layer removal system in the NTF is not currently feasible. The primary issues addressed in the current research are to understand the effects of variations in size and shape of the non-metric model mounting geometry, or standoff; and to eliminate the undesirable thermal gradients present in the balance housing during cryogenic operations. An Energy Efficient Transport (EET) model was used initially and for the majority of the semi-span test technique development work. The most recent semi-span research was conducted using a Boeing 777-200 model. This paper provides a summary of results obtained and lessons learned from these low-speed, semi-span investigations in the NTF.

### Nomenclature

AF	axial force
b	wing span, in.
$C_D$	drag coefficient
$C_L$	lift coefficient
$C_m$	pitching-moment coefficient
$C_p$	pressure coefficient
EET	Energy Efficient Transport
L.E.	leading edge
$M_\infty$	freestream Mach number
NF	normal force
NTF	National Transonic Facility
PM	pitching moment
$P_T$	total pressure, psia
$q_\infty$	freestream dynamic pressure, psf
$R_c$	Reynolds number based on c, where $c = 0.1(\text{test section area})^{0.5}$
$R_{\bar{c}}$	Reynolds number based on mean geometric chord
RM	rolling moment
T.E.	trailing edge
$T_T$	total temperature, °F
X/L	longitudinal distance from fuselage nose nondimensionalized by fuselage length
$\alpha$	angle of attack, deg
2-D	two-dimensional
3-D	three-dimensional

### Test Facility

The NTF<sup>6</sup> is a unique national facility that provides high Reynolds number test capability for vehicles (such as commercial transport airplanes) designed to fly in and through the transonic speed regime. The

NTF is a conventional closed-circuit, fan-driven wind tunnel that is capable of operating at elevated pressures and cryogenic temperatures to obtain high Reynolds numbers. The test section is 8.2 by 8.2 by 25 ft and has a slotted floor and ceiling. In addition, turbulence is reduced by four damping screens in the settling chamber and a contraction ratio of 15 to 1 from the settling chamber to the nozzle throat. Fan-noise effects are minimized by acoustic treatment both upstream and downstream of the fan.

The NTF has an operating pressure range of approximately 15 to 125 psia, a temperature range of -260 to 150°F, and a Mach number range of 0.2 to 1.2. The maximum Reynolds number per foot is  $146 \times 10^6$  at Mach 1. The test gas may be either dry air or nitrogen. When the tunnel is operated cryogenically, heat is removed by the evaporation of liquid nitrogen, which is sprayed into the tunnel circuit upstream of the fan. During this operational mode, venting is necessary to maintain a constant total pressure. When air is the test gas, heat is removed from the system by a water-cooled heat exchanger at the upstream end of the settling chamber. Further tunnel details and facility information are provided in reference 7.

When conducting semi-span model investigations a sidewall model support system, as illustrated in figure 2, is employed. The sidewall model support system is installed in the test section wall, but must be removed when full-span, sting mounted model investigations are conducted. The semi-span model is mounted on the tunnel wall midway between the floor and ceiling, 13 ft aft of the beginning of the test section, and is attached via adaptive hardware to the semi-span balance. The non-metric model mounting geometry, or standoff, is mounted to a wall turntable plate and rotates with the model and balance as angle of attack is set. Heaters and a thermal insulator are present within the balance housing as a means by which to keep the balance near room temperature. Further details of the model support system will be presented later when cryogenic testing issues are addressed.

### EET Model Investigations

#### Model Description

The semi-span model first investigated in the NTF and used for the majority of the test technique development investigations was an Energy Efficient Transport (EET)<sup>8</sup> configuration. This semi-span

model incorporated the port wing from an existing and previously tested full-span EET model. A half-fuselage and multiple standoff geometries, which were used to offset the semi-span model from the wind tunnel wall, were fabricated for use with the existing port wing. The EET model was chosen for the semi-span development effort because an existing wing could be used, and a previously generated full-span data set was also available for use as a baseline for comparison. Although the full-span data set was generated over 15 years prior and in a different wind tunnel, it did provide a reasonable point from which to begin. The EET full-span data which will be used for comparison purposes in this paper was obtained from references 8 and 9.

A sketch of the EET semi-span model as initially tested in the NTF is shown in figure 3. The fuselage was 6.2 ft long and had a maximum diameter of 8.62 in. The wing had an aspect ratio of 10, a leading-edge sweep angle of 28.8 degrees, and employed a supercritical airfoil with a four-element high-lift system. The high-lift system consisted of a full-span, leading-edge slat and part-span, trailing-edge, doubled-slotted flaps. No vertical or horizontal tails were used in the investigations. A wing reference area and reference geometric chord of 2.189 ft<sup>2</sup> and 8.401 in., respectively, were used in the calculations of force and moment coefficients. The model was instrumented with pressure orifices at span stations A and B on the wing as well as on the half-fuselage as illustrated in figure 3. A flow-through engine nacelle was used on all configurations unless otherwise noted. The moment reference center was located 40.44 in. aft of the fuselage nose.

### Initial Standoff Investigation

#### Standoff Description

In the initial investigation a simple two-dimensional (2-D) standoff shape was chosen as a reasonable place to begin for semi-span test technique development. The 2-D shape used consisted of a simple 2-D extension of the fuselage symmetry plane. The standoff height was on the order of the fuselage radius, which in turn positioned the semi-span model just outside the wall boundary layer. In this initial semi-span model installation a teflon strip seal was employed between the metric half-fuselage and the non-metric standoff to serve as a flow blocker for the nominal 0.20-in. gap between the model parts.

In addition to the original 2-D standoff, a three-dimensionally (3-D) shaped standoff, which was a mirror image of the half-fuselage, was also tested. Both 2-D and 3-D standoff shapes were the same height and are shown together for comparison in figure 3.

### Experimental Results

Initially, small white tufts were placed on the wind tunnel wall in a simple 1- by 1-in. grid around the nose of the standoff in order to gain insight into the flowfield behavior in this region. Images showing streamline patterns from the tuft flow visualizations are presented in figure 4 for both 2-D and 3-D standoff geometries. The visualization for the 2-D standoff geometry indicates the sidewall boundary layer separates just upstream of the model, and a horseshoe vortex is formed in the juncture region between the 2-D standoff and the tunnel wall. This would be expected as a stagnation point must exist on the leading edge of the 2-D standoff. Similar results, using oil flow visualization on a semi-span model with a 2-D standoff, are presented in reference 3. Tuft flow visualization for the 3-D standoff geometry shows no evidence of flow separation on the sidewall, and thus indicates a flowfield which appears much more representative of that for a full-span model.

Longitudinal force and moment data for the EET semi-span model with both 2-D and 3-D standoff geometries are presented together for comparison along with the baseline full-span data set in figure 5. This initial full-span to semi-span comparison clearly indicates differences between the two data sets, but it also indicates that the 3-D standoff delays the stall angle of attack on the semi-span model by approximately 2 degrees, thereby improving the correlation with the full-span data set. Surface pressure data at wing station A, although not presented herein, also indicate that the 3-D standoff results in an improved correlation with full-span data over that from the 2-D standoff. After this initial 2-D and 3-D standoff study, it was concluded that a 3-D shaping of the standoff would likely provide a beneficial means by which to improve correlation of semi-span data with full-span data.

### Investigation with Reduced Standoff Height

At this point in the development of the semi-span test technique, attention was directed toward the

question of standoff height. A computational study was underway to assess the effects of variations in standoff height, and results from these studies are presented in reference 4. The fundamental conclusion drawn from the computational work was that the best correlation between semi-span data, with a 2-D standoff, and full-span data resulted when the standoff height was equal to twice the tunnel sidewall boundary layer displacement thickness ( $\delta^*$ ). This analysis was conducted for a freestream Mach number of 0.2 and a Reynolds number, based on reference geometric chord, of 4.2 million. These were the conditions being run for the semi-span model so as to match the conditions of the existing full-span data set.

#### Standoff Description

As a result of the conclusions from the computational study, a standoff was built that would offset the semi-span model from the tunnel wall a distance equal to twice the sidewall boundary layer displacement thickness ( $2\delta^*$ ). Both a 2-D and 3-D standoff were built and tested for this standoff height. The 3-D standoff had a simple undercut leading and trailing edge. Both of these standoffs are presented in a sketch in figure 6. The undercut sections had a parabolic shape and extended approximately 10 in. aft of the leading edge and approximately 20 in. forward of the trailing edge. A photograph of the semi-span EET model with the 2-D,  $2\delta^*$  standoff is presented in figure 7.

In addition to the features of the new standoff, some other new features were incorporated into the model at this time. Model flexibility had been a problem in the previous wind tunnel investigation to the extent that the low-pressure region on the outboard side of the half-fuselage would draw the fiberglass half-fuselage away from the standoff enough to allow the teflon strip seal between the two to become dislodged. In order to reduce model flexibility, the new standoffs, as well as a new half-fuselage, were fabricated using a composite graphite material. The seal between the fuselage and the standoff was also improved. A labyrinth-type seal was incorporated in this region to minimize any flow between the metric half-fuselage and the non-metric standoff. An electrical fouling circuit was also a part of this seal to ensure there would be no contact, or fouling, between the fuselage and standoff.

#### Experimental Results

Longitudinal force and moment data for the semi-span model with the 2-D,  $2\delta^*$  standoff geometry are presented for comparison with the baseline full-span data set in figure 8. Correlation between full-span and semi-span data in terms of lift-curve slope and drag coefficient is good. Pitching-moment data agree quite well from 4 to approximately 10 degrees angle of attack, but then do not agree well beyond that. The stall behavior between full-span and semi-span models is essentially reproduced. Generally, semi-span data with the  $2\delta^*$  standoff correlate better with the full-span data than that of data with the larger standoff, as was presented earlier in figure 5.

Longitudinal force and moment data for the semi-span model, illustrating the effects of the standoff undercut leading and trailing edges relative to the 2-D standoff, are presented in figure 9. Testing of the undercut standoff configuration was limited to a Reynolds number of  $2.8 \times 10^6$  due to fouling at the nose between the non-metric standoff and metric fuselage. This fouling resulted from inadequate stiffness of the thinner, undercut standoff leading edge, which deflected under aerodynamic load. Undercutting the standoff leading edge had only small effects on the aerodynamic data. A positive increment in pitching moment is noted for angles of attack above 6 degrees, and a slight increase in drag coefficient is evident across the angle of attack range. The effects of undercutting the standoff trailing edge were practically undetectable in the longitudinal data. In order to gain further insight into the effects of undercutting the standoff leading and trailing edges, fuselage pressure data were obtained. Pressure distributions are presented at three fuselage stations in figure 10. The data presented at fuselage station 12 indicate that an undercut standoff leading edge will generate a flow acceleration over the top of the fuselage at that location. The data presented at fuselage station 24 indicate that an undercut standoff leading edge will have almost no effect on the fuselage surface pressure at that location. The data presented near the aft end of the fuselage at station 72 show no effects at all due to either an undercut standoff leading or trailing edge. When the fuselage pressure data are compared with the longitudinal data of figure 9, it would suggest that the nose-up increment in pitching moment due to the undercut standoff leading edge is a result of the flow acceleration noted on the top of the fuselage at station 12.

Results of the 28\* standoff investigation indicate that this standoff height will produce semi-span data which correlate better with full-span data than that from a semi-span configuration with a standoff height on the order of the wall boundary layer height. The ratio of standoff height (1 in.) to semi-span (39.71 in.) for this configuration is 0.025. This ratio is presented to provide a means of comparison between this model and the larger 777 semi-span model that will be discussed later. The effects of undercutting the standoff leading and trailing edges are shown to be small; however, this may well be a direct result of the much smaller standoff height than was tested previously. The effects noted due to the standoff undercut leading edge, although small, still indicate that standoff shaping shows promise as a means by which to improve correlation of semi-span data with full-span data.

#### Labyrinth Seal Description

An additional part of the investigation included assessing the effects of sealing the gap between the fuselage and the standoff. This issue presents conflicting requirements in that a completely airtight seal is most desirable aerodynamically; however, there still must be no contact, or fouling, between the metric fuselage and the non-metric standoff. As a result of this a labyrinth seal has been used. A sketch illustrating the labyrinth seal used between the fuselage and the standoff is presented in figure 11. The fuselage side of the labyrinth seal was fabricated directly as an integral part of the flat side of the fuselage. However, in order to simplify the fabrication of the standoff this side of the labyrinth seal was made independently and then attached to the standoff. This independent piece also provided an opportunity to obtain data with it removed, and thus assess any potential need at all for a seal in this area.

#### Experimental Results

When investigating effectiveness of the labyrinth seal, the first logical step was to determine if there was any amount of flow at all passing between the fuselage and the standoff. This was determined by assessing the pressure data from six pressure orifices located on the fuselage centerline on the flat, or back, side of the fuselage. Data were obtained with the labyrinth seal in its nominal configuration, which consisted of a 0.20-in. gap between the fuselage and the standoff (see figure 11), and data were also obtained with the gap between the fuselage and the standoff completely taped over. These pressure data are presented in

figure 12(a), and show that there is some flow leakage past the labyrinth seal near fuselage station 30. The next step was to reduce the gap between the fuselage and the standoff to see if flow leakage in this area could be reduced. Data are presented in figure 12(b) for the nominal 0.20-in. gap and for a reduced gap of 0.10 in. This 0.10-in. gap was the smallest possible without developing substantial fouling problems. These data indicate that reducing the gap resulted in only small effects. Even though the data presented show evidence of flow leakage between the fuselage and the standoff, it should be noted that this did not appear to interfere with the aerodynamics of the high-lift wing.

Since some flow between the fuselage and the standoff did exist, and it was not creating a detrimental effect, there was interest in determining if a labyrinth seal was really necessary at all. To investigate this, the portion of the labyrinth seal on the standoff was removed and data were obtained. Longitudinal data illustrating effects of the presence of the labyrinth seal are presented in figure 13. These data show that the absence of the labyrinth seal produces small effects until the stall angle of attack is reached. At this point it is shown that the model will stall at a lower angle of attack when the labyrinth seal is not present. Further insight into effects of the presence of the labyrinth seal is found in the fuselage pressure data presented in figure 14. These data indicate that at an angle of attack of 12.84 degrees the absence of the labyrinth seal has essentially no effect. Although data are presented only at fuselage station 12, no effect was noted along the entire length of the fuselage at this angle of attack. When the angle of attack is increased to near the stall angle, removal of the labyrinth seal results in less accelerated flow around the fuselage. This is noted in the data presented for fuselage stations 12 and 24. These results support the trend noted in the force and moment data (figure 13) in that an adequate seal between the fuselage and the standoff is important in the region of maximum lift.

Results of investigating the effects of the labyrinth seal indicate that a labyrinth seal which minimizes flow between the fuselage and the standoff is necessary, especially when testing in the region of maximum lift. However, some limited flow between the fuselage and standoff is acceptable.

#### Cryogenic Operation

All semi-span data presented to this point have been for testing in the NTF in the air mode. In an

effort to minimize the expense of the semi-span test technique development investigations, it was decided that the studies needed to understand the effects of standoff height and shape and sealing between the fuselage and the standoff would not need to be conducted in the much more expensive nitrogen mode of operation. However, in order to obtain data at flight Reynolds numbers, testing in the nitrogen mode of operation is required.

To begin the discussion of thermal effects on the balance during cryogenic operation, further description of the model support system, which identifies the main elements and their function, will now be provided. The NTF semi-span model support system, also referred to from this point forward as the mechanism, is a completely self-contained system that includes the angle of attack drive mechanism and the force balance. A sketch of the system showing it installed on the test section wall has previously been presented in figure 2. The fully assembled mechanism has a total weight of 10,000 pounds. The mechanism is installed behind the NTF sidewall, within the tunnel plenum. It is used exclusively for semi-span testing and is not present during other NTF testing configurations. Due to the removable design of this model support system, the entire package must be compact to allow for installation and removal. The original design of the system was based on the concept of cryogenic balance operation. Heaters within the mechanism were installed for the primary purpose of maintaining an acceptable operational temperature of the angle of attack drive system and bearings. The NTF-114S force balance is housed within the mechanism and is connected to the model by an insulating spacer, a strut, and a model-specific adapter.

#### Balance Description

The NTF-114S is a monolithic balance, shown in figure 15(a), and is made from 18-percent nickel maraging steel. Its overall dimensions are 16 in. in diameter by 25.75 in. long, and it weighs 950 pounds. It is a five component balance measuring normal force, axial force, pitching moment, rolling moment, and yawing moment. The balance instrumentation consists of a primary and secondary set of strain gage bridges, which provides a completely redundant set of component measurements. The balance temperature profile is monitored by 52 platinum resistive temperature detectors (RTDs). These temperature sensors are located on the balance to provide a global temperature profile as well as localized measurements near the strain gages. The balance also contains an

on-board accelerometer which provides an absolute reference of balance pitch attitude. The full-scale balance capacity and calibration accuracies are provided in figure 15(b). The balance was originally fabricated, instrumented and calibrated for cryogenic operation; however, actual operation of the balance was later determined to be at ambient temperature regardless of the tunnel test section temperature. This balance cavity ambient temperature resulted from the operation of multiple heaters required for the mechanical operation of the mechanism and will be discussed in more detail in the following paragraphs. The performance of the balance has been verified with the tunnel in warm air mode. A sample of the repeatability of the balance measurements is illustrated by three repeat polar sequences (a sweep of angle of attack) in figure 16.

#### Cryogenic Operation Issues

During the first cryogenic excursions performed using the semi-span mechanism, operational difficulties in setting the angle of attack were revealed. The heater system was inadequate in maintaining the temperature of the drive system. Another more significant result of the early testing was the temperature profile of the balance. Although the heaters were designed to maintain the temperature of the mechanism drive system, they also unintentionally heated the balance. Due to the inherent complexity of the mechanism design, it was considered unlikely that modifications to the mechanism could allow the balance to operate at cryogenic temperatures, as originally intended. Therefore, a "hot balance" concept was adopted. This "hot balance" concept is unique to the operation of NTF balances. All other NTF balances are designed and calibrated for cryogenic operation. This new concept of temperature isolation from the test conditions as compared to temperature equilibrium with the test conditions has proven to be a challenging aspect in development of the NTF semi-span test capability.

Once the operational issues with the model support system were resolved, efforts were focused on balance data quality during cryogenic operations. Under these conditions, the balance structure experienced large temperature gradients which deteriorated data quality. It is important to note that thermal gradients on the strain gaged measuring elements of the balance generate real strain, which is indistinguishable from the strain generated by an applied load. There are also secondary localized convection effects

on the strain gages themselves, but these were not the primary source of error in the balance measurements.

The following three areas of balance performance were investigated as a result of the first aerodynamic tests to quantify the balance data quality. First, the aerodynamic data and the wind-off zeroes were less repeatable during cryogenic tunnel operations as compared to warm tunnel operations. This can be seen by comparing the results of three repeat polar sequences during warm operations (figure 16) to the same sequences during initial cryogenic operations (figure 17). These data clearly showed a degradation in data repeatability during cryogenic operations. Second, the balance temperature gradients changed rapidly during a polar sequence as shown in figure 18. The change in the gradient within a single polar sequence was as much as 35°F. This change occurred within approximately five minutes and indicates a significant amount of heat transfer from the large mass of the balance. Also, repeated polar sequences had a cumulative effect on the magnitude of the balance temperature gradients. For comparison purposes it should be noted that during the warm air mode of operation, the balance cavity and the test section remained at ambient temperature; thus, no significant temperature gradients existed on the balance. Third, the heaters located in close proximity to the balance were not controlled to their design set point of 75°F; see figure 19. In fact, balance housing heater element temperatures reached 240°F, which created a 490°F differential temperature between the gas temperature in the test section and the surface temperature of the heaters within the mechanism, which are in close proximity to the balance. As a result of this first investigation, the balance data quality was determined to be unacceptable and an effort was launched to improve the balance thermal environment.

#### Corrective Actions

The initiative to correct the thermal gradient effects focused on two primary hypotheses of the physical process involved that induced the thermal gradients on the balance. The first hypothesis was based on gas from the plenum passing through the mechanism to the tunnel test section as depicted in figure 20. This flow would be induced by a negative differential pressure located at the model-to-balance interface. The second hypothesis was based on the actual flow field around the model generating a re-circulating flow path in and out of the balance cavity. In both cases, a complete seal between the balance cavity and the tunnel test

section would block the flow path; but, this would not be acceptable in terms of balance data quality because it would create a parallel load path, or foul, across the metric end of the balance to the non-metric support structure. Since a positive contacting seal could not be installed, a combination of active and passive sealing was therefore implemented.

A comprehensive redesign of the mechanical, electrical, and control systems of the semi-span mechanism was performed and implemented.<sup>10</sup> The balance cavity was sealed as a pressure tight vessel from the plenum in order to eliminate the flow of gas through the mechanism. This required installation of rubber seals on the non-metric end of the mechanism, plugging all holes used for electrical wiring, and a complete redesign of the instrumentation connection panel that incorporated pressure tight bulkhead connectors. Additional non-contacting seals were installed behind the tunnel wall on the model strut and adapter to block the re-circulating flow path. Also, new cover shields were installed on the balance to block any flow that might breach the new seals. These new cover shields completely encased the measurement flexures by a labyrinth arrangement with a minimum gap of .050 in. The balance was also temperature compensated to a tighter tolerance and calibrated within its new warm operating temperature range. A final temperature control improvement added was an active gaseous nitrogen purge system. This system supplies warm nitrogen gas into the balance cavity through five equally spaced holes around the circumference of the non-metric end of the balance. Purge gas temperature and mass flow rate are externally monitored and adjusted by a closed loop control system. This control system also incorporates zone control over the radiant heater elements within the balance cavity. All of these improvements are illustrated in figure 21.

#### Experimental Results

The installation of these seals was performed in an incremental manner and the resultant improvement in balance temperature gradients is illustrated in figure 22. This plot illustrates the correlation between the change in the differential temperature from the top of the balance to the bottom as a function of the model angle of attack within a single polar sequence (note: a positive differential temperature indicates that the top is warmer than the bottom). This figure contains four configurations of the sealing devices as follows: configuration 1 is the data from the first cryogenic

entry and has no seals installed; configuration 2 has seals in all locations except the model instrumentation hole and on the model strut and adapter; configuration 3 adds the model instrumentation hole seal; and configuration 4 includes the seals on the model strut and adapter, and the active purge system.

When the data from configuration 2 are examined, the balance temperature profile is found to be slightly improved as compared to the first tunnel entry; however, a sizable balance temperature gradient is still present. After much painstaking investigation into the possible remaining paths for flow into the balance cavity, it was determined that the hole in the model fuselage, through which the model instrumentation passes, should be sealed. This hole was tightly plugged and the resultant balance temperature profile indicated a flat response to the change in angle of attack. Even though the temperature gradient did not change with angle of attack in configuration 3, a stable temperature gradient still existed. Configuration 4 includes the seals on the model strut and adapter, and the use of the active gaseous nitrogen purge. Results from the installation of all the seals and the purge system provided excellent temperature stability of the balance. Therefore, the corrective actions were demonstrated to be successful in eliminating the thermal gradients on the balance within a polar sequence.

### 777 Model Investigation

#### Model Description

A 5.2-percent scale 777-200 semi-span model was designed and built specifically for testing at the NTF such that data could be obtained for the first time up to flight Reynolds number for takeoff and approach conditions. This model was also built with multiple standoff geometries in order to provide further opportunity to improve upon the semi-span test capability. This 5.2-percent scale model was intended to have the same external geometry as a 6.3-percent scale, full-span model previously tested in the DERA 5-Meter tunnel, and a 4.2-percent scale, full-span model previously tested in the Ames 12-Foot PWT. As a result, data from the 6.3- and 4.2-percent full-span models<sup>11</sup> will be used as a baseline data set for comparison with the semi-span data.

A photograph of the model as it was tested in the NTF test section is presented in figure 23. The fuselage was 10.7 ft long and had a maximum

diameter of 13.11 in. The wing had an aspect ratio of 8.421, a quarter-chord sweep angle of 31.64 degrees, and a semi-span ( $b/2$ ) of 61.438 in. No vertical or horizontal tails were used for the data presented in this paper. Both takeoff and landing wing configurations were tested; however, only the takeoff wing configuration was used during the semi-span test technique development portion of the investigation. The wing leading edge configuration consisted of inboard and outboard slats, with a seal Krueger between the flow-through engine nacelle and inboard slat. The trailing edge configuration included a double-slotted inboard flap, flap, flap, outboard single-slotted flap, and aileron. The model was instrumented with six chord-wise rows of pressure taps on the wing, as well as substantial pressure tap coverage on the half-fuselage. All pressure tap locations were chosen to match those existing on the previously tested 4.2-percent 777-200 full-span model.

#### Standoff Description

The standoff components were designed such that two standoff heights and three standoff leading-edge shapes could be tested. A 1-inch and a 2-inch standoff, which would position the half-fuselage one or two inches respectively away from the tunnel sidewall, were investigated. The 1-inch standoff, which positions the half-fuselage a distance of twice the sidewall boundary layer displacement thickness away from the wall, was expected to provide better correlation with full-span data than the 2-inch standoff based on previous results. However, the use of a larger standoff was expected to provide benefits when standoff shaping was investigated due to an increased surface area with which to work. Three leading-edge shapes: a 2-D, a filleted, and an undercut, as illustrated in figure 24, were investigated at each standoff height. The filleted and undercut leading edges were computationally designed<sup>12</sup> to alleviate the sidewall boundary layer separation, and thus reduce or eliminate the formation of the horseshoe vortex that forms around the leading edge of a 2-D standoff. Therefore it was anticipated that a filleted or undercut leading edge would improve correlation with full-span data. The shaping of the filleted and undercut leading edges extended aft 20 percent of the fuselage length. A labyrinth seal was used between the metric half-fuselage and the non-metric standoff. A spring-loaded teflon seal was used on the backside of the standoff to maintain a constant seal between the standoff and the wind tunnel wall.

## Experimental Results

Longitudinal data are presented for the 777 semi-span model with both 1-inch and 2-inch standoffs with 2-D leading edges in figure 25. When these data are compared with the DERA full-span data, it is noted that the configuration with the 2-inch standoff provides a slightly better correlation with the full-span data set when lift and pitching moment coefficients are compared. An increase in standoff height is shown to produce an increase in lift curve slope as has been noted in previous studies.<sup>3</sup> It is more difficult to identify which standoff configuration provides a better correlation with the full-span drag coefficient data since the correlation with full-span data varies for both configurations over the angle-of-attack range. At low to moderate angles of attack, data from the 2-inch standoff configuration correlates slightly better with the full-span drag data, while at higher angles of attack data from the 1-inch standoff configuration correlates better. Based on all the longitudinal data, therefore, it was decided that the 2-inch standoff configuration provided a better overall correlation with full-span data. The ratio of standoff height to semi-span for the 2-inch standoff configuration is 0.033. Recalling that this same ratio for the EET semi-span model (1-inch standoff) was 0.025 indicates that a standoff on the order of approximately 3 percent of the model semi-span will provide NTF semi-span data which correlates better with full-span data than that resulting from other standoff heights. It is anticipated that a 3-D shaping of the standoff could further improve correlation of semi-span data with full-span data.

It is noted that the post-stall semi-span data do not correlate well with the full-span data. The substantial nose-up pitching moment associated with the abrupt post-stall lift loss is not believed to be a real effect. Whether this is attributed to model or wind tunnel differences or something else is unknown.

In order to investigate the effects of standoff leading edge shaping, both a filleted and an undercut standoff leading edge were tested, and the results for the 2-inch standoff are presented in figure 26. These data indicate very little effect of leading edge shaping on lift and pitching-moment coefficient. Differences are noted, however, when drag coefficient data are compared for the different leading edges. As revealed in previous research, an undercut standoff leading edge results in an increased drag coefficient when compared to the 2-D leading edge. This potentially results from the reduced velocity of the flow around the forward portion of the half-fuselage, which occurs

when the freestream flow at the nose of the model has an additional flow path between the undercut standoff nose and the wind tunnel wall. The same trends were observed when the filleted and undercut leading edges were investigated on the 1-inch standoff.

To gain a more detailed insight into the effects of standoff leading edge shaping, surface pressure data were obtained on the half-fuselage for each standoff leading edge configuration tested. These pressure data were obtained from pressure taps located longitudinally around the fuselage, just slightly to the port side of the fuselage symmetry plane. These data were in turn compared with the same fuselage pressure data obtained on the 4.2-percent full-span model. The purpose here was to determine which standoff leading edge configuration would produce fuselage pressure data on the semi-span model which best matched the full-span fuselage pressure data. Fuselage centerline pressure data for each of the three standoff leading-edge configurations are presented together for comparison with the 4.2-percent full-span fuselage pressure data in figure 27. No tare and interference corrections were applied to the full-span data; therefore, the effects of the vertical bi-pod model support system have not been removed. This causes two effects which must be noted when the full-span and semi-span data are compared. First, pressure data on the bottom of the fuselage is directly affected by the bi-pod support and thus would not be expected to match the semi-span data; and second, the presence of the bi-pod support increases the effective angle of attack of the full-span configuration by approximately one degree;<sup>11</sup> therefore, the full-span data presented are for an indicated angle of attack of one degree less than that of the semi-span data. The effects of the standoff leading-edge shaping are primarily noted in the upper surface fuselage pressure data at the locations of X/L between 0.04 and 0.2. In this area the 2-D standoff leading edge is shown to produce data that correlates better with full-span data than data from the fillet or undercut configurations. Up to this point in our research it was expected that the 2-D standoff leading edge would be least desirable due to the presence of a horseshoe vortex. These pressure data, however, show that the efforts to eliminate the presence of the horseshoe vortex do not improve the correlation of semi-span data with full-span data. Therefore the presence of a horseshoe vortex around the standoff leading edge may not necessarily be undesirable as originally expected. The goal is to have the same pressure distribution on the half-fuselage as that on the full-span fuselage, regardless of what is happening in the flowfield over the standoff, and of

the three standoff leading-edge shapes tested, the 2-D leading edge provides the best correlation.

### Cryogenic Operation

Thermal stability of the balance during cryogenic operations was well controlled during the 777 semi-span investigation. This was expected based on the results presented in figure 22 illustrating the effectiveness of the final seals and purge system from the last EET semi-span investigation. Even though the last configuration of the sidewall model support system was effective in controlling the thermal environment of the balance, some additional improvements were made prior to the 777 semi-span investigation. These improvements included adding a purge gas flow path through the center of the balance, and replacing the model strut and adapter seals with more robust and precisely fabricated seals.

Cryogenic data obtained during three repeat polar sequences are presented together for comparison in figure 28. These data indicate very good data repeatability, and thus very good balance cavity thermal control. In order to compare data repeatability for data obtained under cryogenic operations to that of data obtained in air, a final plot was prepared which includes three repeat runs for each condition. These data are presented in figure 29. The delta values represent the difference between the data point at a given angle of attack and the average data value at that angle of attack. The solid lines represent the 95-percent confidence interval of the finite data sample. The 95-percent confidence interval can be interpreted as the bounds about the estimated mean that encompass the true mean value, with a chance of 95-percent. A more in-depth description of the confidence interval and the methods used to calculate it are presented in references 13 and 14. Examination of the data from figure 29 reveals that the repeatability of the cryogenic runs is just as good as that for the air runs, thus indicating an elimination of the varying thermal gradients on the balance. It is noted that due to the inherent dynamics of the flow at and beyond the stall angle of attack, the 95-percent confidence interval expands greatly, as expected, at these conditions.

### Conclusions

Multiple investigations have been conducted in the National Transonic Facility at the NASA Langley Research Center in which a semi-span transport configuration and the sidewall model support system have been tested with multiple parametric variations to

support the development of a viable semi-span testing technique. The results of these investigations are presented as follows:

1. A standoff height on the order of 3 percent of the model semi-span will provide much better correlation of semi-span data with full-span data than a standoff height on the order of the height of the wall boundary layer.
2. An undercut standoff leading edge will alleviate the separation of the sidewall boundary layer that occurs with a 2-D standoff leading edge. However, a 2-D standoff leading edge produced fuselage pressure data in the nose region which correlated better with full-span data than that from a filleted or undercut standoff leading edge.
3. Standoff shaping shows promise as a means by which to improve correlation of semi-span data with full-span data, although the effects are reduced as standoff height is reduced. An undercut standoff leading edge produced an increase in drag as compared to a 2-D standoff leading edge.
4. A seal which minimizes flow between the fuselage and standoff is necessary, especially when testing in the region of maximum lift. A labyrinth-type seal, which did allow some limited flow between the fuselage and standoff, was found to be acceptable.
5. Improvements to the sidewall model support mechanism, which include multiple seals and a purge gas system, have effectively reduced temperature gradients on the balance during cryogenic operation. This provided balance performance at the same level as that obtained during air operation.

### Acknowledgments

A large number of people contributed to the success of the NTF wind tunnel investigations discussed in this paper. The authors would like to express their thanks and appreciation for the efforts of the Semi-Span Test Techniques Research Team, the staff of the NTF, and The Boeing Company.

### References

1. Lynch, F. T.: Experimental Necessities for Subsonic Transport Configuration Development. AIAA 92-0158, January 1992.

2. Viehweger, G.; and Ewald, B.: Half Model Testing in the Cologne Cryogenic Tunnel (KKK). AIAA 94-2511, June 1994.
3. Gatlin, G. M.; and McGhee, R. J.: Experimental Investigation of Semispan Model Testing Techniques. *Journal of Aircraft*, Vol. 34, No. 4, 1997, pp. 500-505.
4. Milholen II, W. E.; Chokani, N.; and McGhee, R. J.: Development of Semispan Model Test Techniques. *Journal of Aircraft*, Vol. 33, No. 6, 1996, pp. 1115-1122.
5. Earnshaw, P. B.; Green, A. R.; Hardy, B. C.; and Jelly, A. H.: A Study of the use of Half-Models in High-Lift Wind-Tunnel Testing. AGARD-CP-515, October 1992, pp. 20.1-20.9.
6. Gloss, B. B.: Current Status and Some Future Test Directions for the US National Transonic Facility. *Wind Tunnels and Wind Tunnel Test Techniques*. R. Aeronaut. Soc., 1992, pp. 3.1-3.7.
7. Fuller, Dennis E.: Guide for Users of the National Transonic Facility. NASA TM-83124, 1981.
8. Morgan, Harry L., Jr.; and Kjelgaard, Scott O.: Low-Speed Tests of a High-Aspect-Ratio, Supercritical-Wing Transport Model Equipped With a High-Lift Flap System in the Langley 4- by 7-Meter and Ames 12-Foot Pressure Tunnels. NASA TP-2097, 1983.
9. Kjelgaard, Scott O.; and Morgan, Harry L., Jr.: Pressure Distribution Data From Tests of 2.29 m (7.5 ft) Span EET High-Lift Transport Aircraft Model in the Ames 12-Foot Pressure Tunnel. NASA TM-84517, 1983.
10. Balakrishna, S.; Kilgore, W. A.; and Butler, D. H.: Temperature Control of External Balances for Semi-Span Models in Cryogenic Tunnels. *Second International Symposium on Strain Gage Balances*, 1999.
11. Payne, F. M.; Wyatt, G. W.; Bogue, D. R.; and Stoner, R. C.: High Reynolds Number Studies of a Boeing 777-200 High Lift Configuration in the NASA ARC 12' Pressure Tunnel and NASA LaRC National Transonic Facility. AIAA 2000-4220, August 2000.
12. Milholen II, William E.: A Design Methodology for Semi-Span Model Mounting Geometries. AIAA 98-0758, January 1998.
13. Coleman, Hugh W.; and Steele, W. Glenn, Jr.: *Experimentation and Uncertainty Analysis for Engineers*. John Wiley & Sons, Inc., 1989.
14. Wahls, R. A.; Adcock, J. B.; Witkowski, D. P.; and Wright, F. L.: A Longitudinal Aerodynamic Data Repeatability Study for a Commercial Transport Model Test in the National Transonic Facility. NASA TP-3522, 1995.

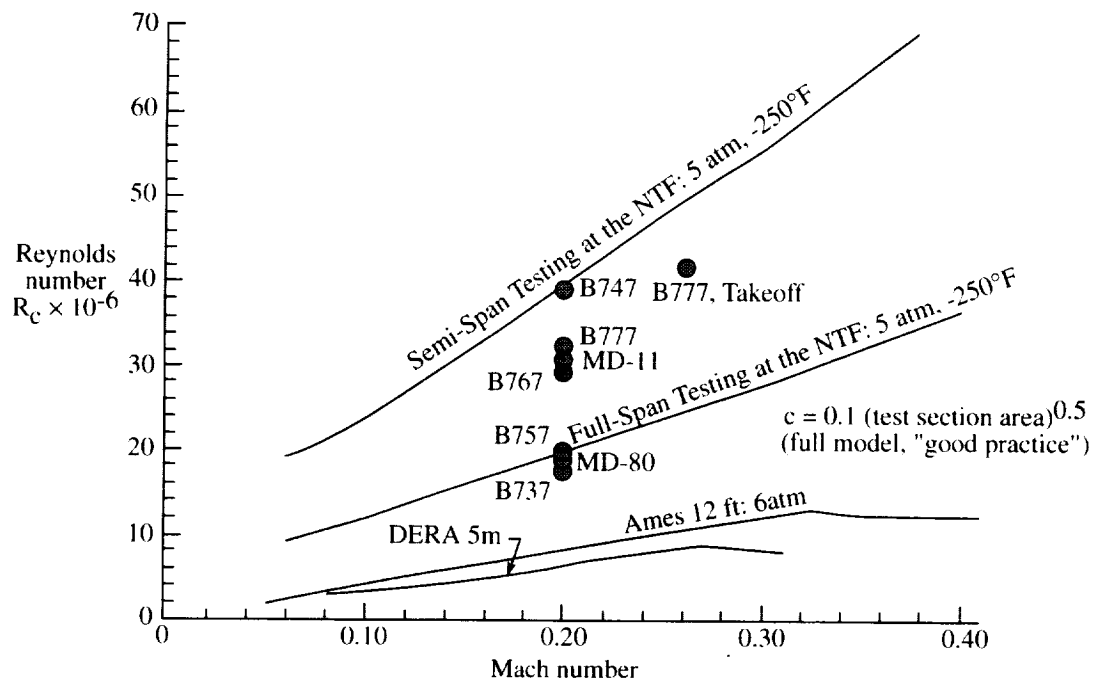


Figure 1. Low speed, high Reynolds number test capabilities.

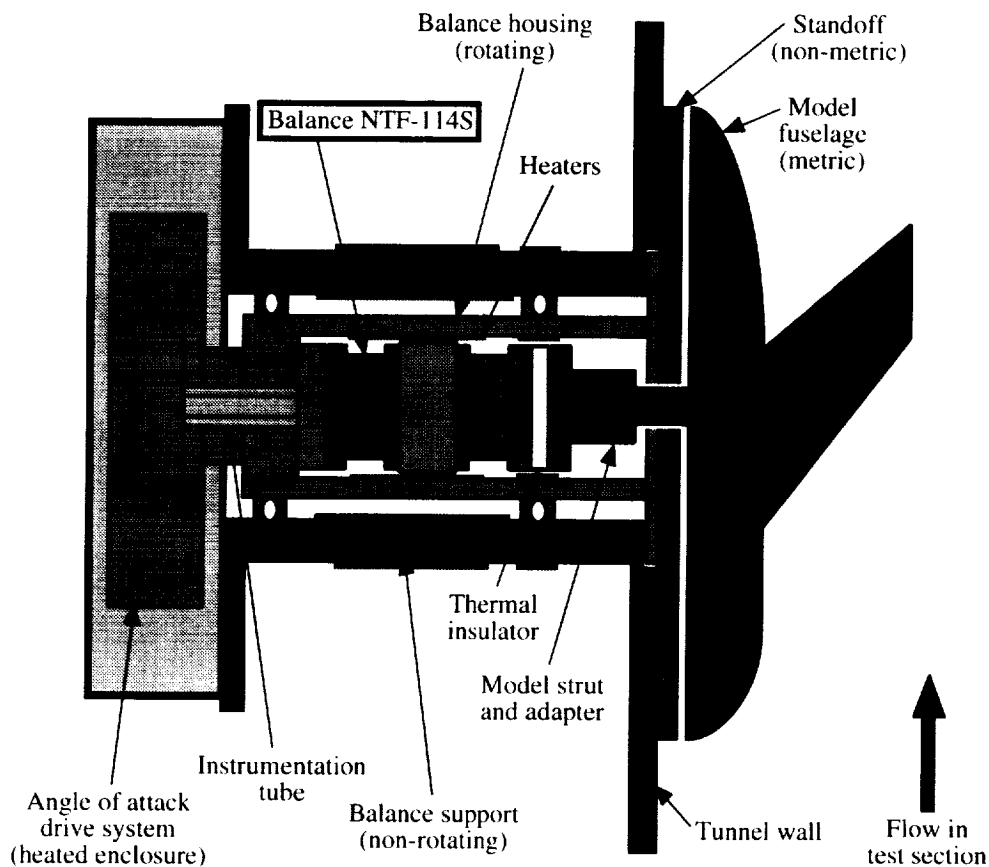
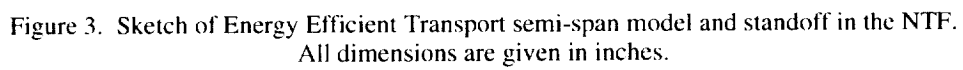
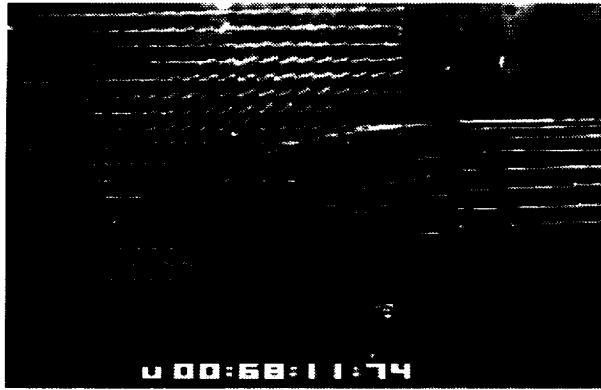
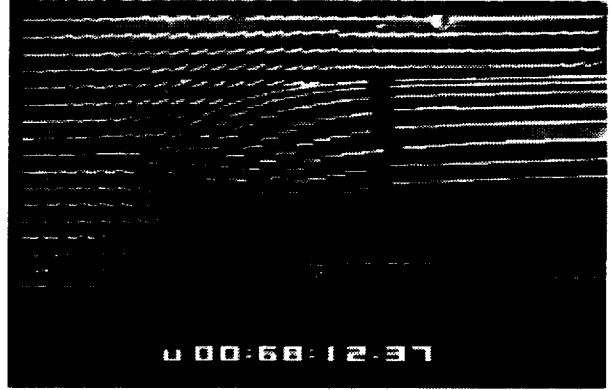


Figure 2. Sketch of sidewall model support system.





2-D Standoff



3-D Standoff

Figure 4. Streamline patterns from tuft flow visualization.  $M_\infty = 0.20$ ,  $R_{\zeta} = 4.2 \times 10^6$ ,  $\alpha = 0^\circ$ .

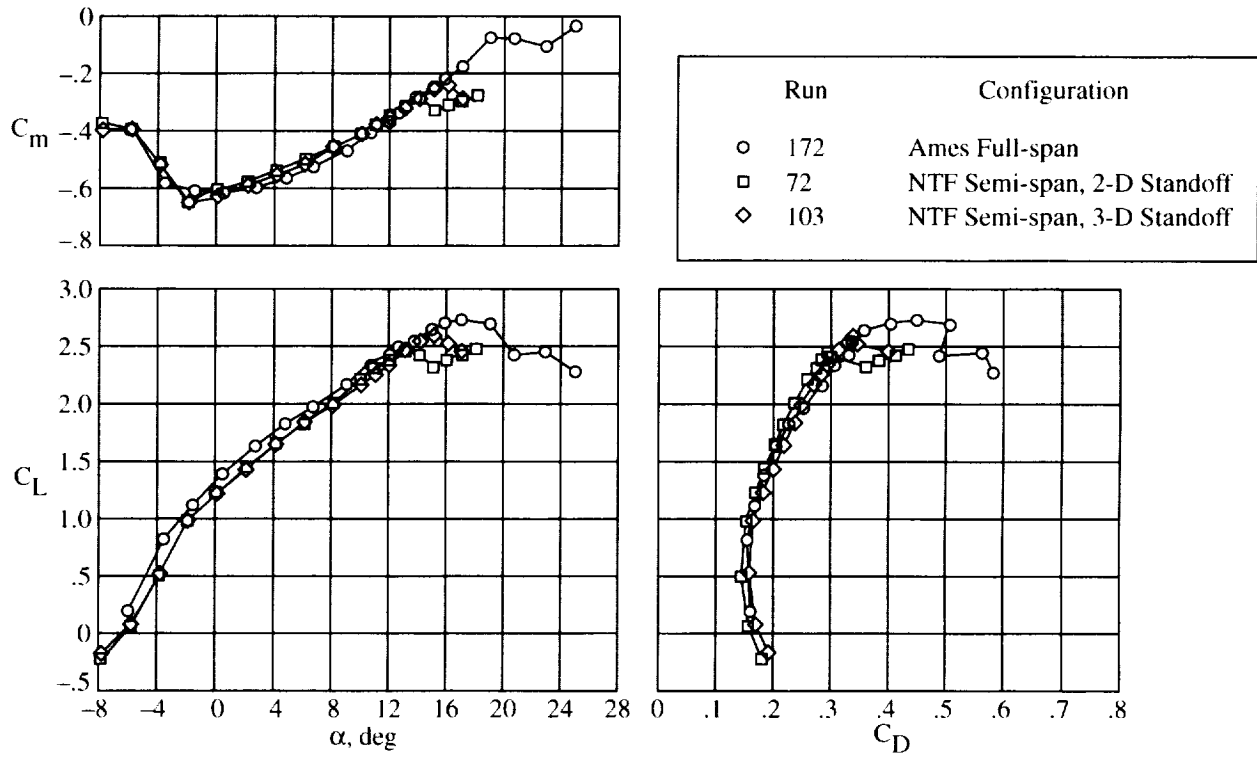


Figure 5. Comparison of full-span and semi-span data. Landing configuration,  $M_\infty = 0.20$ ,  $R_{\zeta} = 4.2 \times 10^6$ .

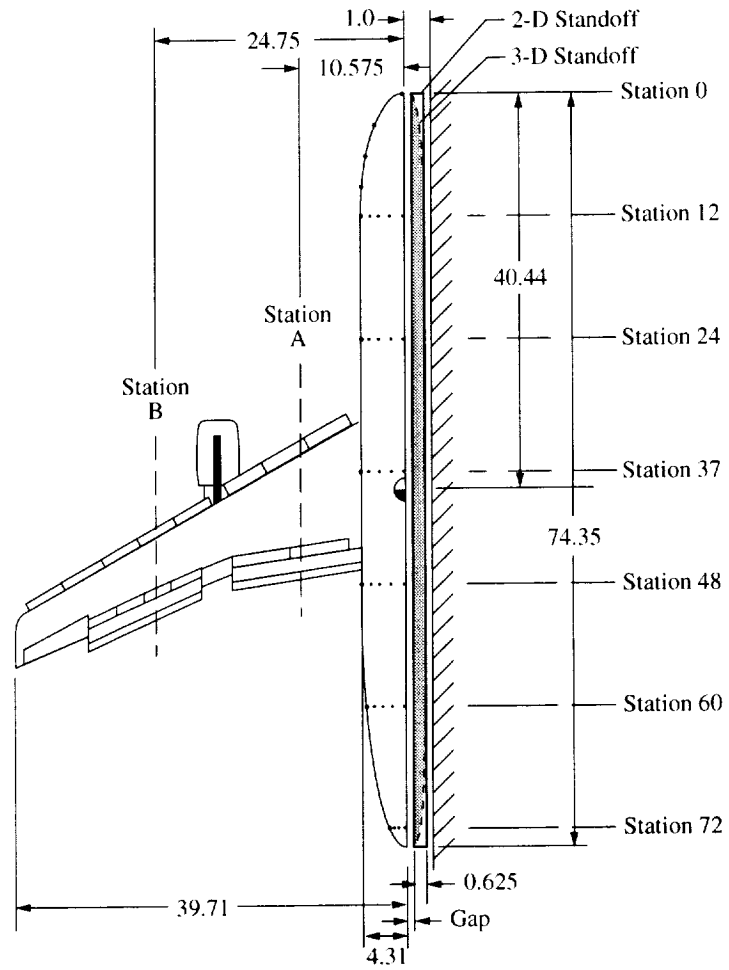


Figure 6. Sketch of EET semi-span model with reduced standoff height. All dimensions are given in inches.

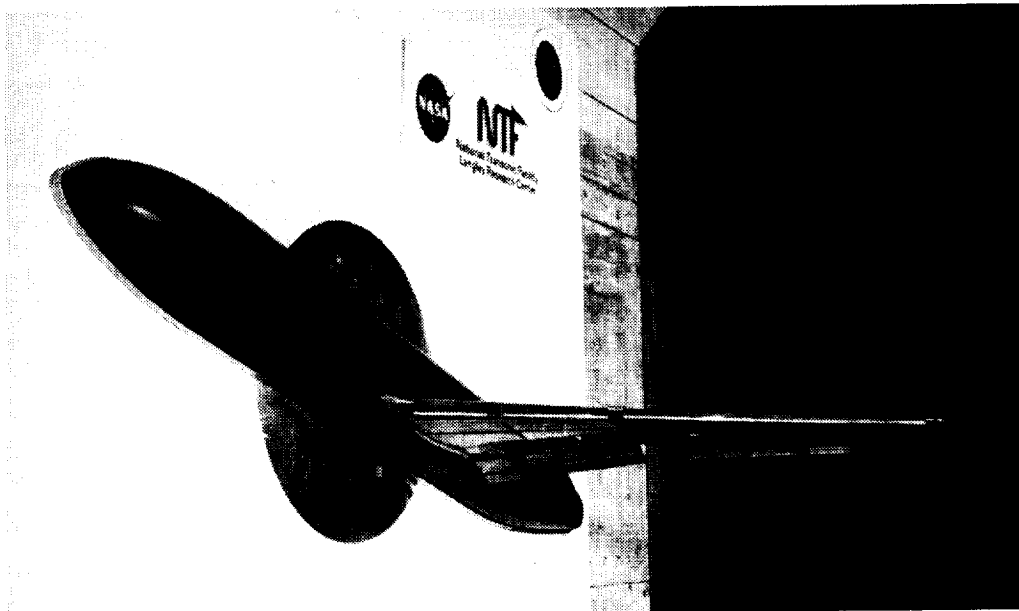


Figure 7. Photograph of takeoff configuration of EET semi-span model in the NTF.

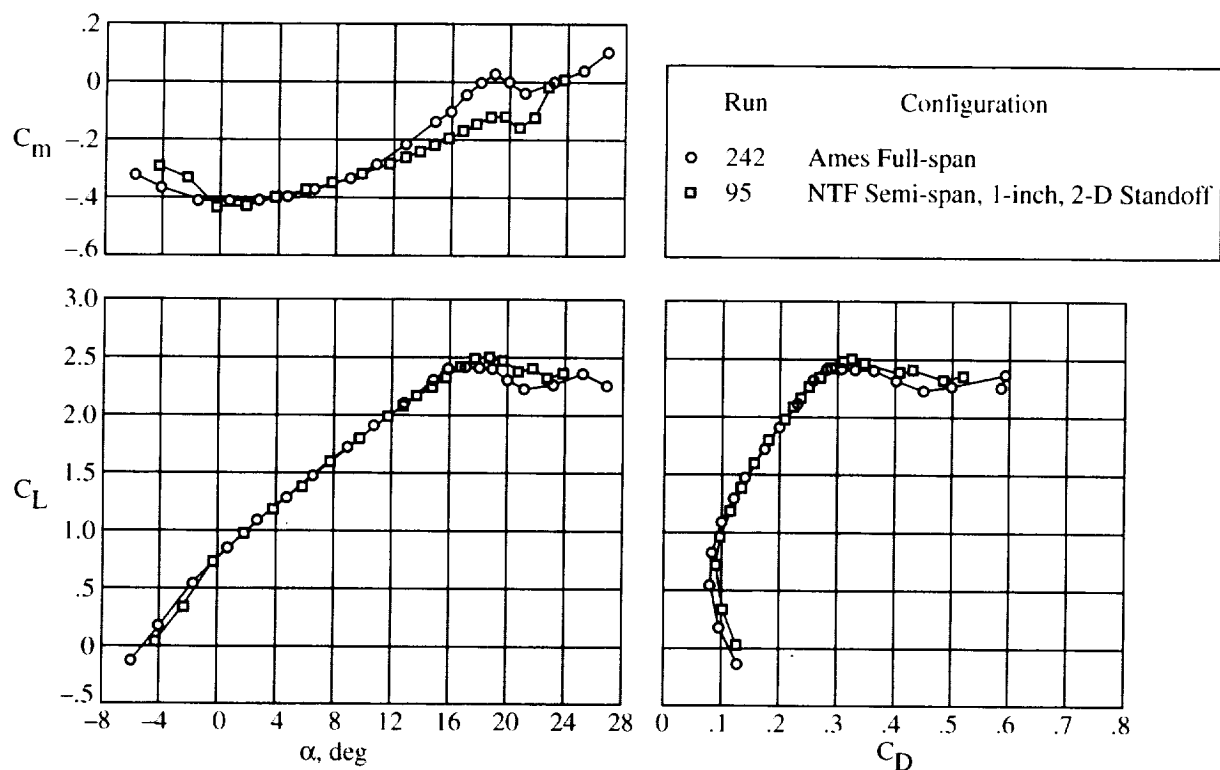


Figure 8. Comparison of full-span and semi-span data. Takeoff configuration,  $M_\infty = 0.20$ ,  $R_c = 4.0 \times 10^6$ .

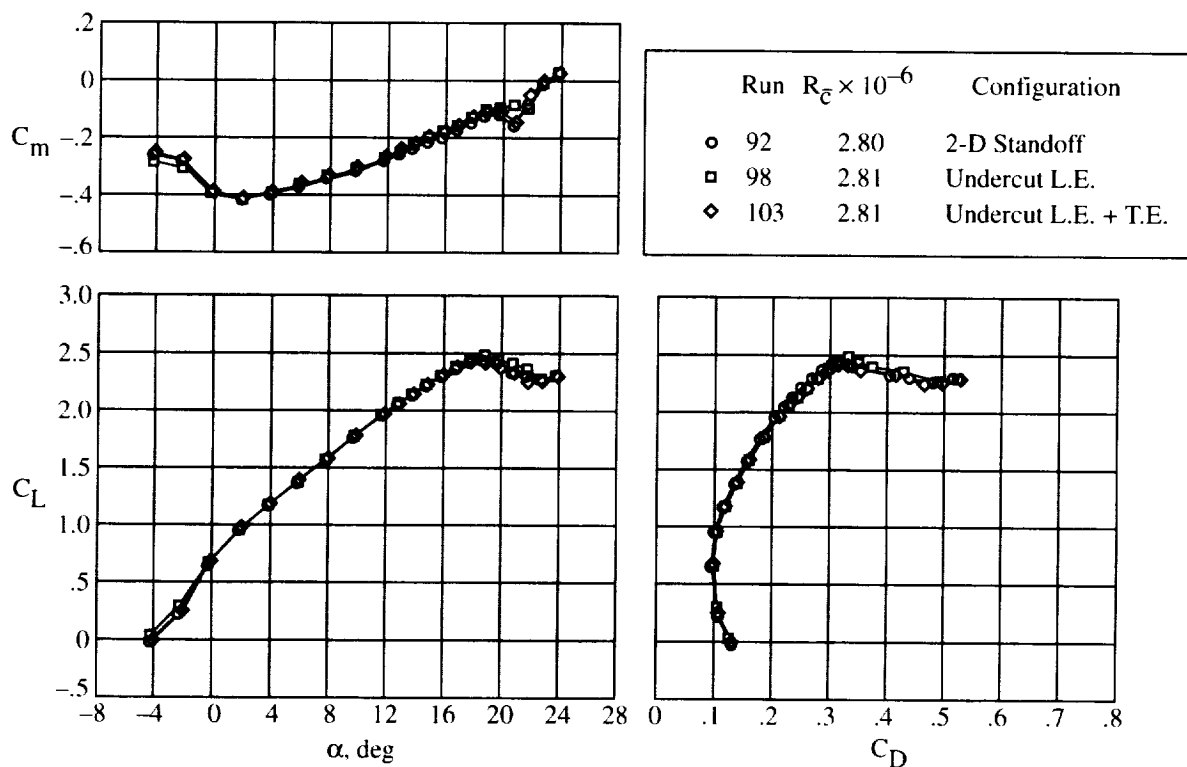
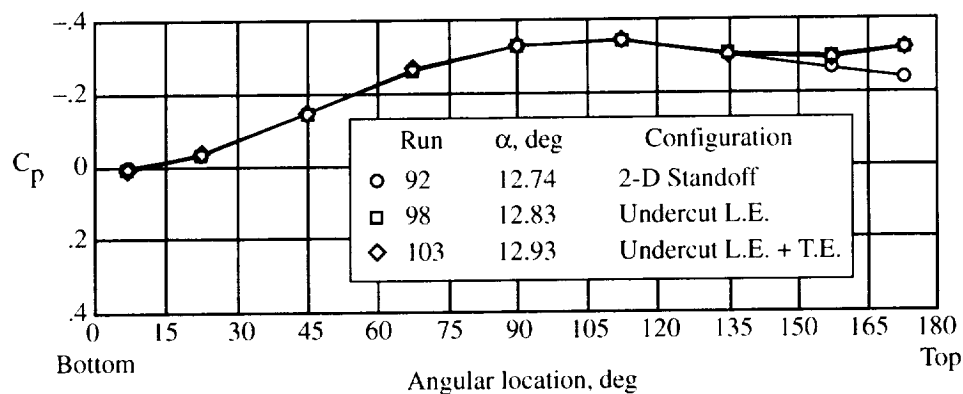
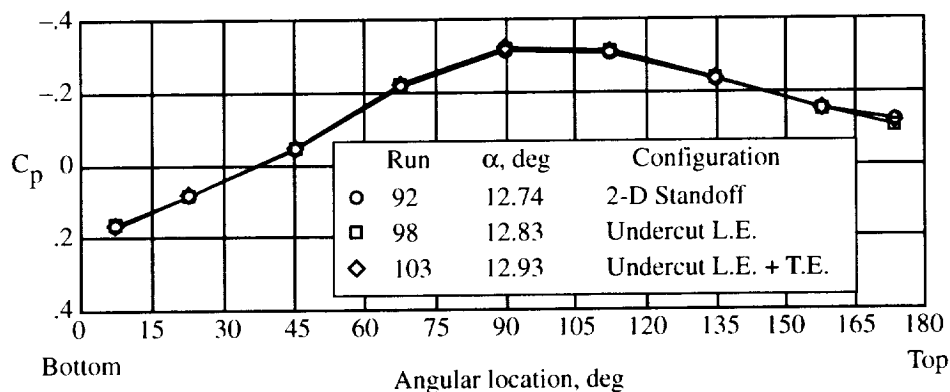


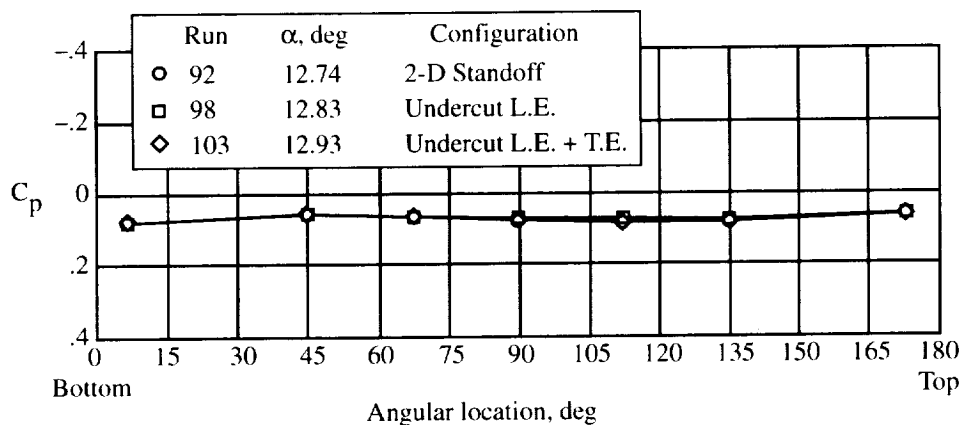
Figure 9. Effect of undercut leading and trailing edges. Takeoff configuration,  $M_\infty = 0.20$ ,  $R_c = 2.8 \times 10^6$ .



(a) Fuselage station 12.



(b) Fuselage station 24.



(c) Fuselage station 72.

Figure 10. Pressure data on fuselage illustrating effects of undercutting the standoff leading and trailing edge.

Takeoff configuration,  $M_\infty = 0.20$ ,  $R_\tau = 2.8 \times 10^6$ .

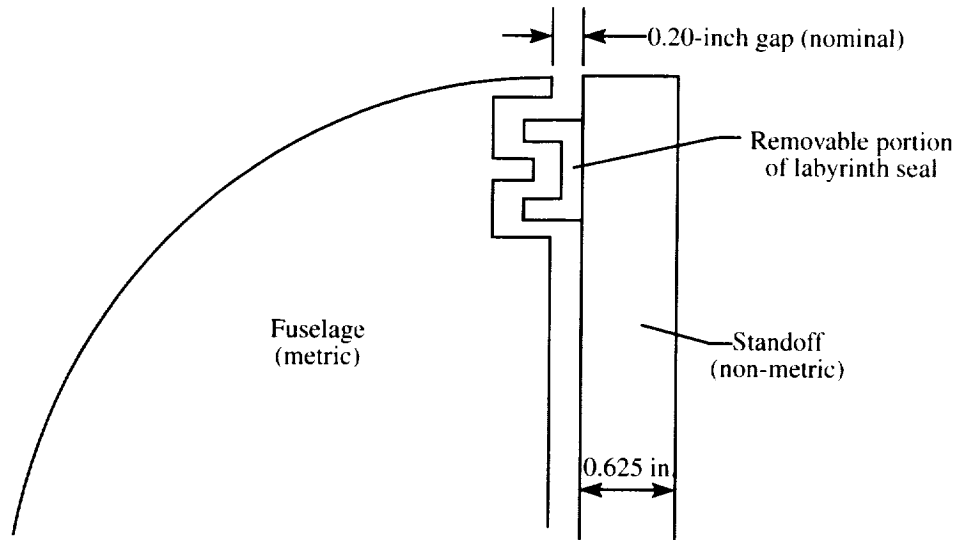
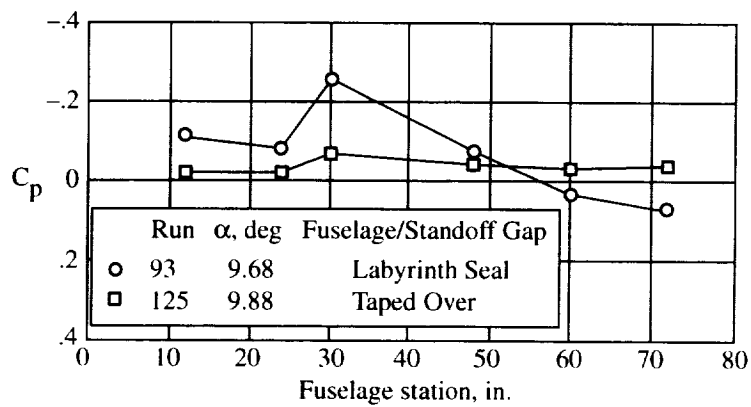
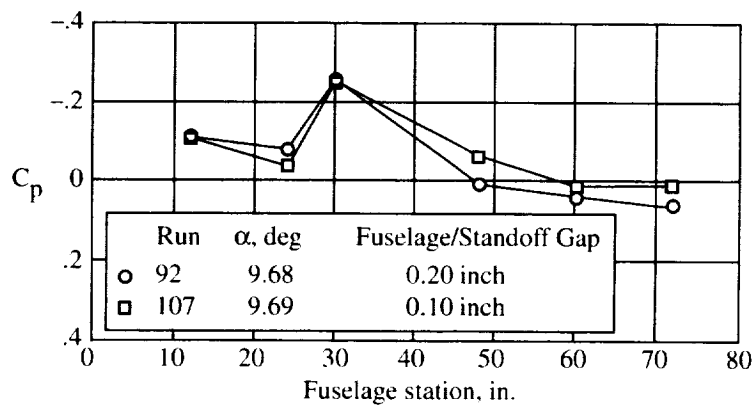


Figure 11. Labyrinth seal between fuselage and standoff.



(a) Effect of complete seal,  $R_{\bar{c}} = 4.2 \times 10^6$ .



(b) Effect of gap size,  $R_{\bar{c}} = 2.8 \times 10^6$ .

Figure 12. Pressure data on internal centerline of fuselage illustrating labyrinth seal performance.  
Takeoff configuration,  $M_{\infty} = 0.20$ .

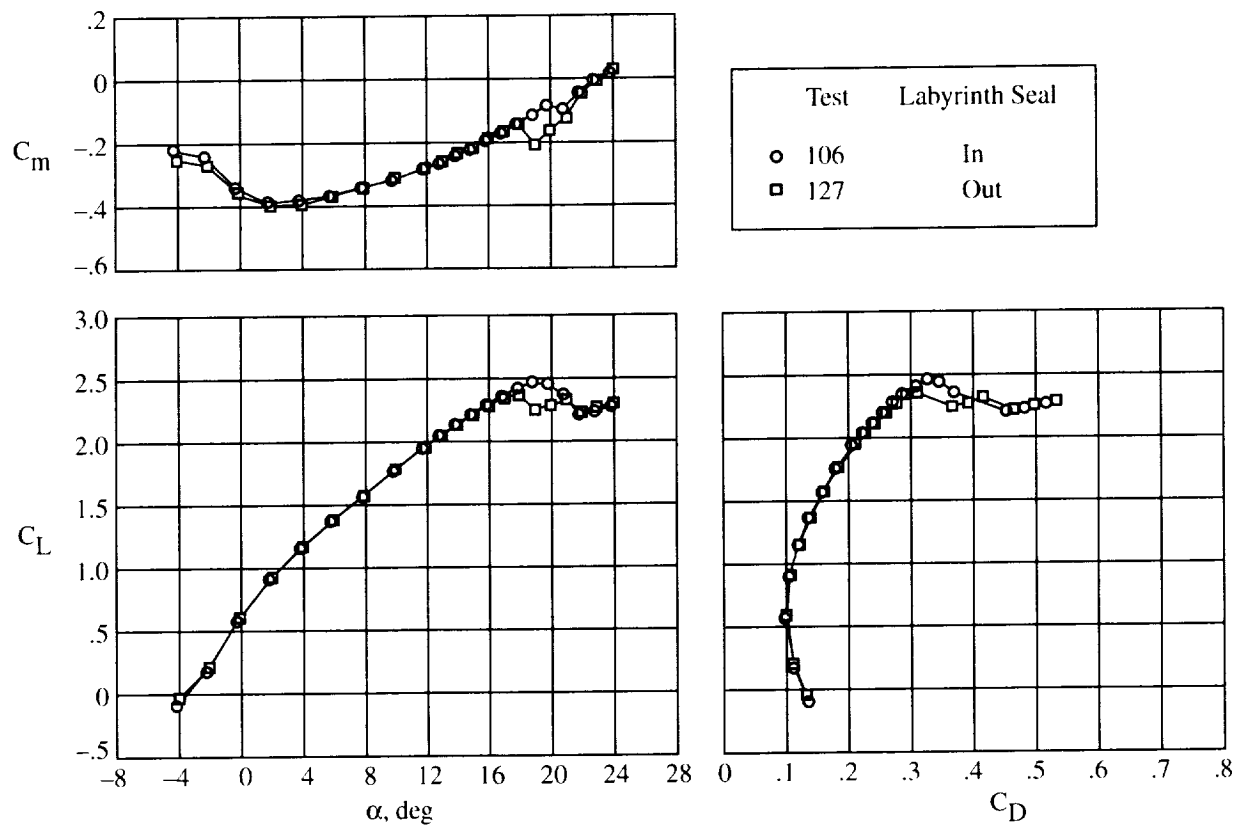
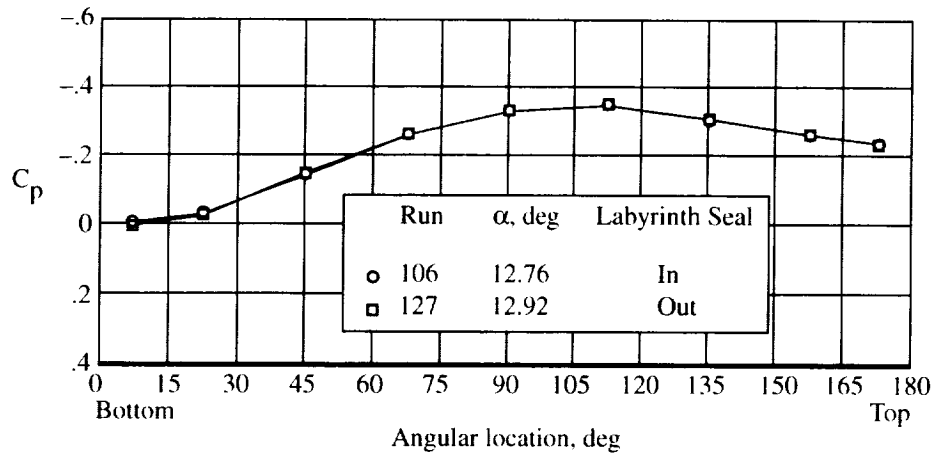
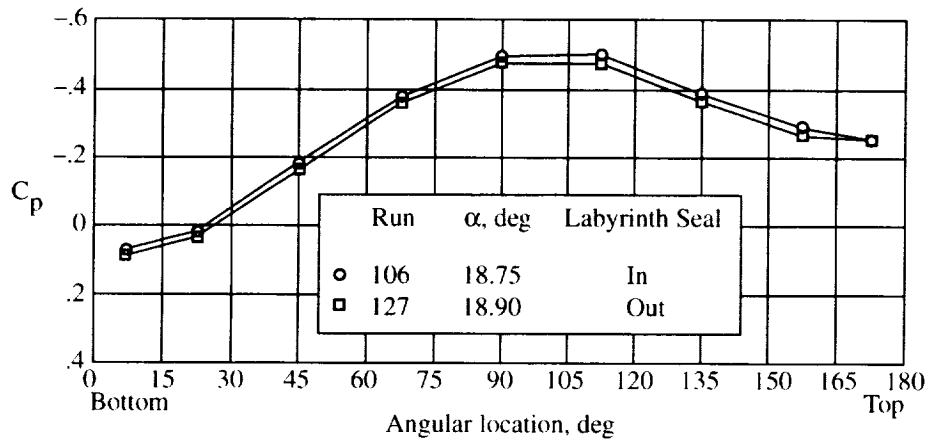


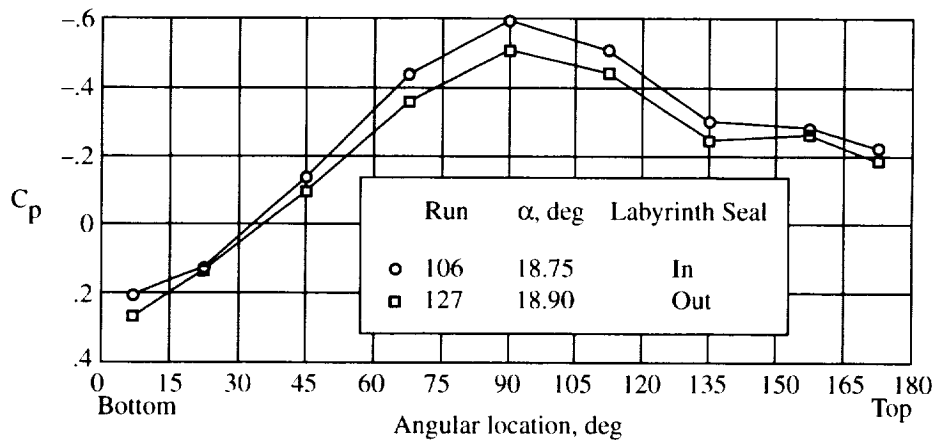
Figure 13. Effect of labyrinth seal. Gap = 0.10 inch, takeoff configuration,  $M_\infty = 0.20$ ,  $R_c^- = 1.6 \times 10^6$ .



(a) Fuselage station 12,  $\alpha = 12.84^\circ$ .



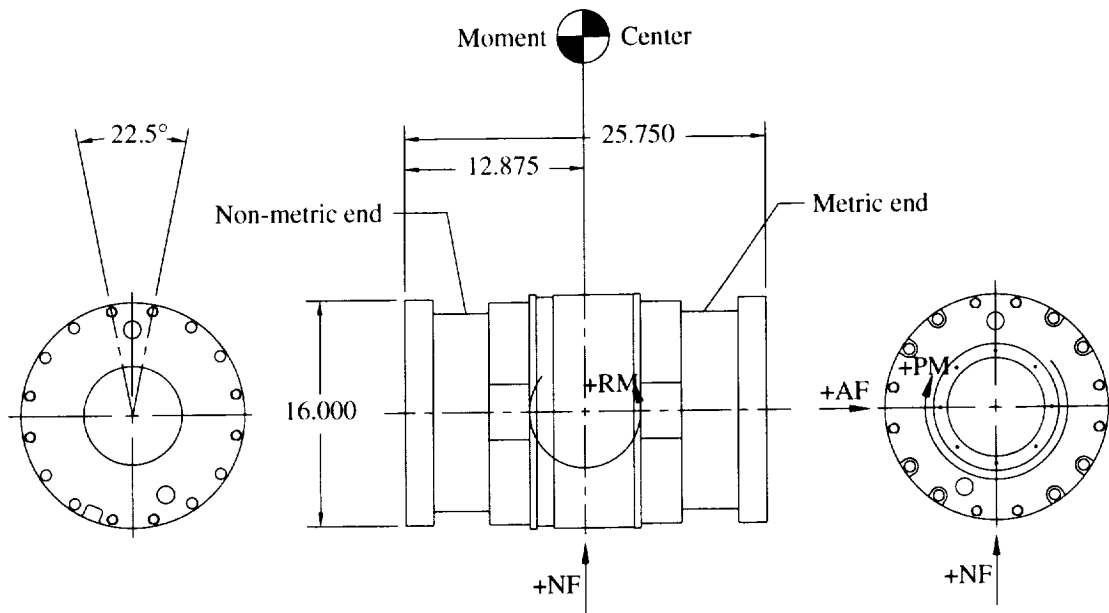
(b) Fuselage station 12,  $\alpha = 18.82^\circ$ .



(c) Fuselage station 24,  $\alpha = 18.82^\circ$ .

Figure 14. Pressure data on fuselage illustrating effects of the labyrinth seal.

Takeoff configuration,  $M_\infty = 0.20$ ,  $R_\zeta = 1.6 \times 10^6$ .



(a) Outline drawing.

Component	Balance Capacity	Accuracy (% of full scale) (95% confidence)
Normal Force	$\pm 6,100$ lbs	0.10
Axial Force	$\pm 1,300$ lbs	0.07
Pitching Moment	$\pm 70,000$ in-lbs	0.06
Rolling Moment	$\pm 353,800$ in-lbs	0.06
Yawing Moment	$\pm 75,400$ in-lbs	0.06

(b) Full-scale balance capacity and calibration accuracies.

Figure 15. NASA Langley Research Center balance NTF-114S. All linear dimensions are given in inches.

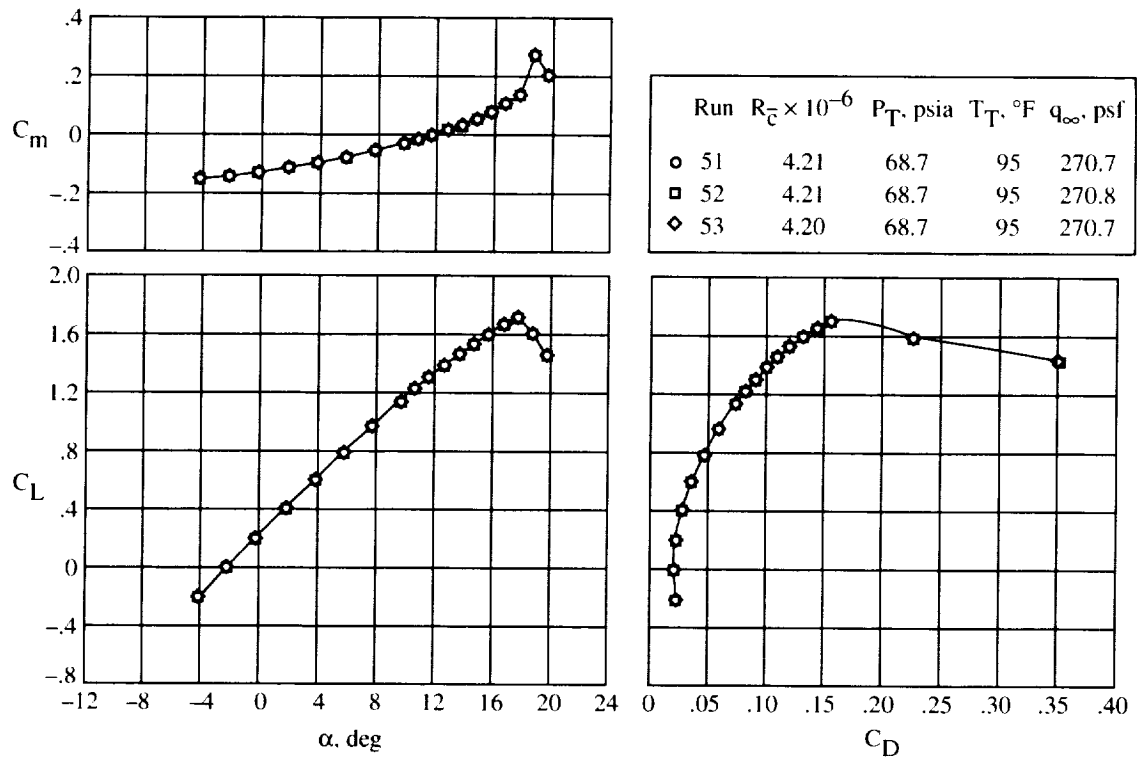


Figure 16. Data repeatability for air mode of operation at 95° F. Cruise configuration,  $M_\infty = 0.20$ , nacelle off.

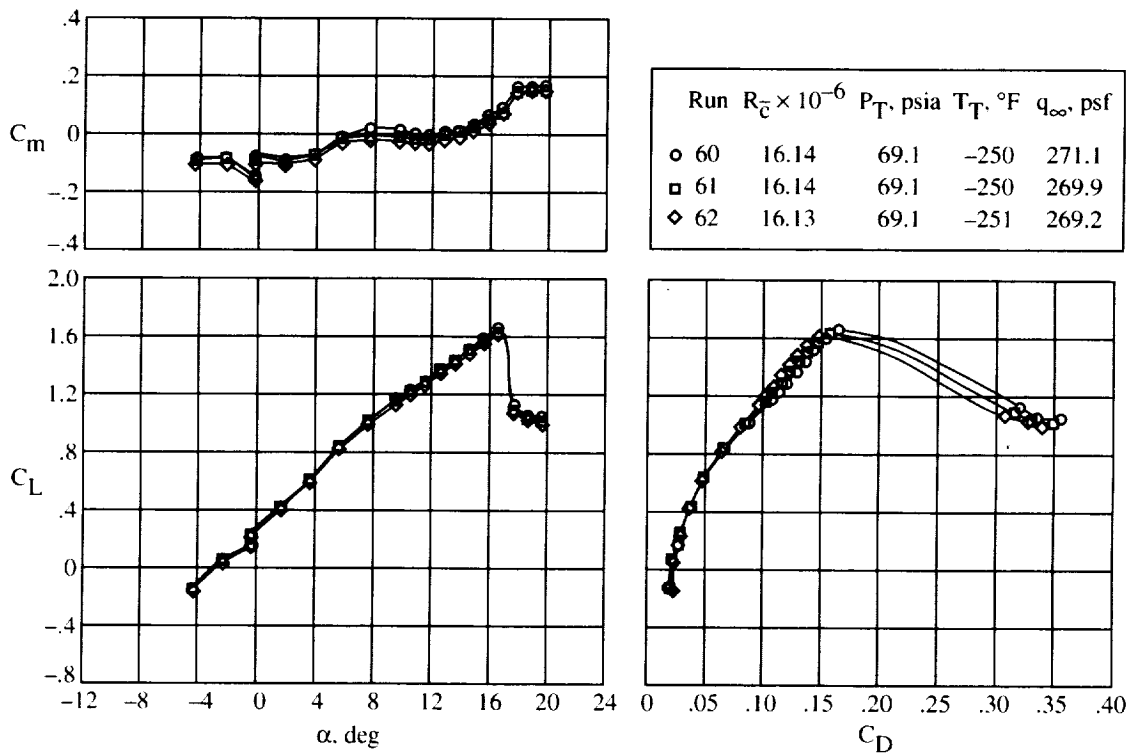


Figure 17. Initial data repeatability for nitrogen mode of operation at -250°F.  
Cruise configuration,  $M_\infty = 0.20$ , nacelle off.

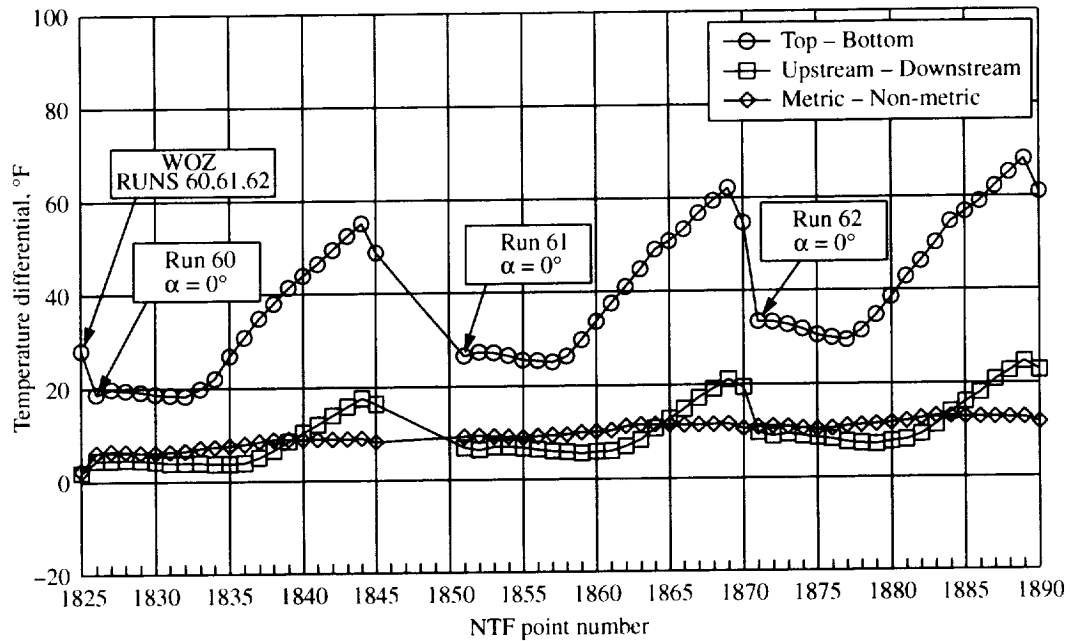


Figure 18. Initial balance temperature differential versus sequential data point.  $P_T = 69$  psia,  $T_T = -250^\circ\text{F}$ .

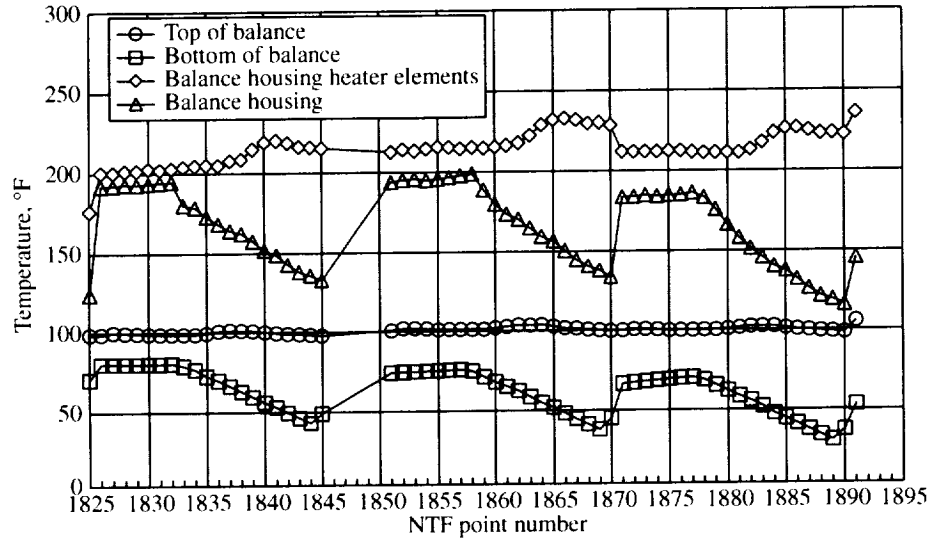


Figure 19. Initial mechanism temperature control versus sequential data point.  $P_T = 69$  psia,  $T_T = -250^\circ\text{F}$ .

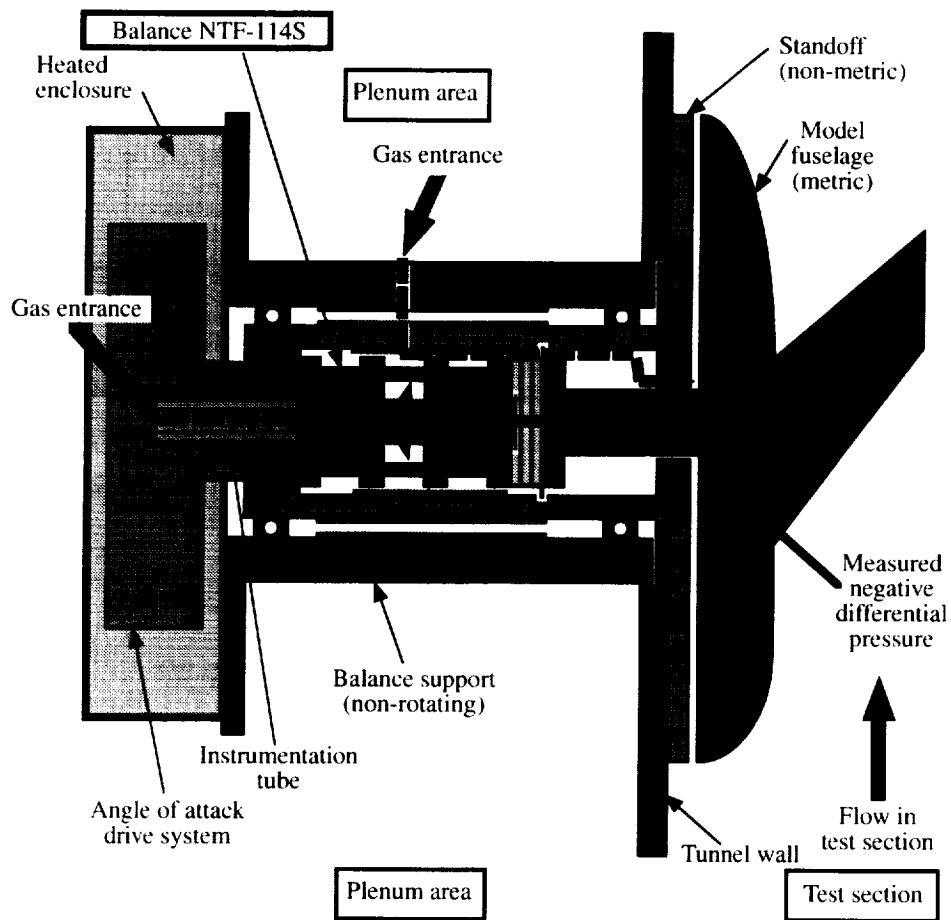


Figure 20. Sketch of flow path of plenum gas to test section.

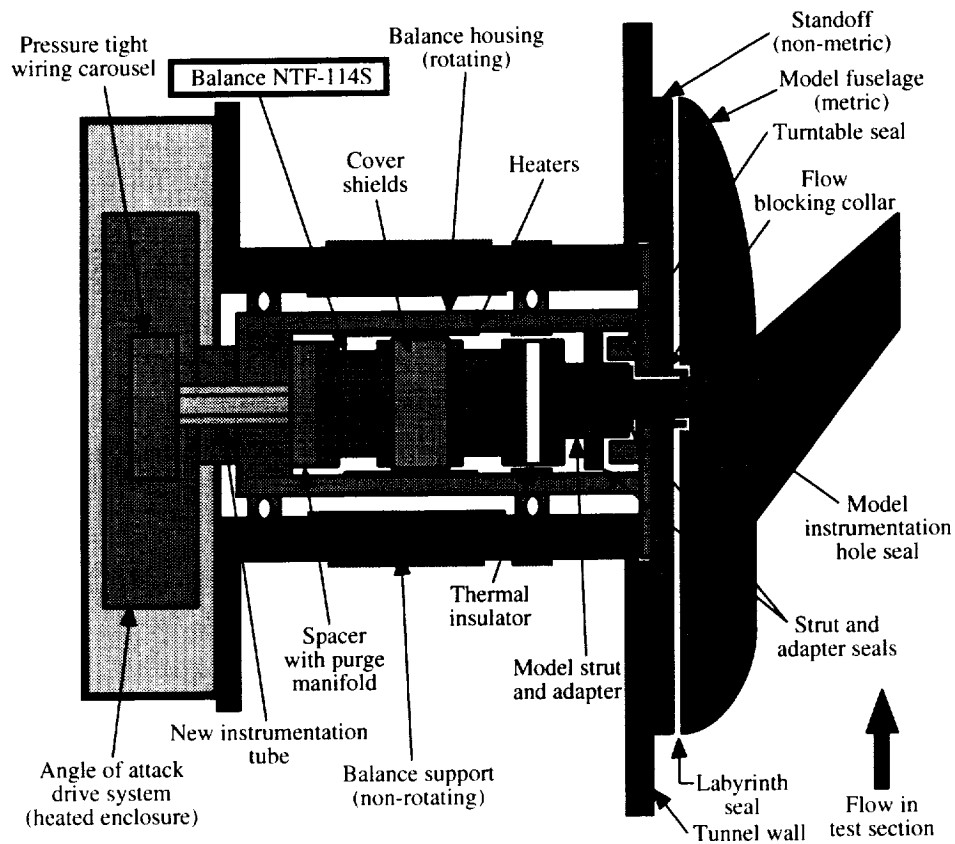


Figure 21. Sketch of modifications to the sidewall model support system to improve cryogenic operations.

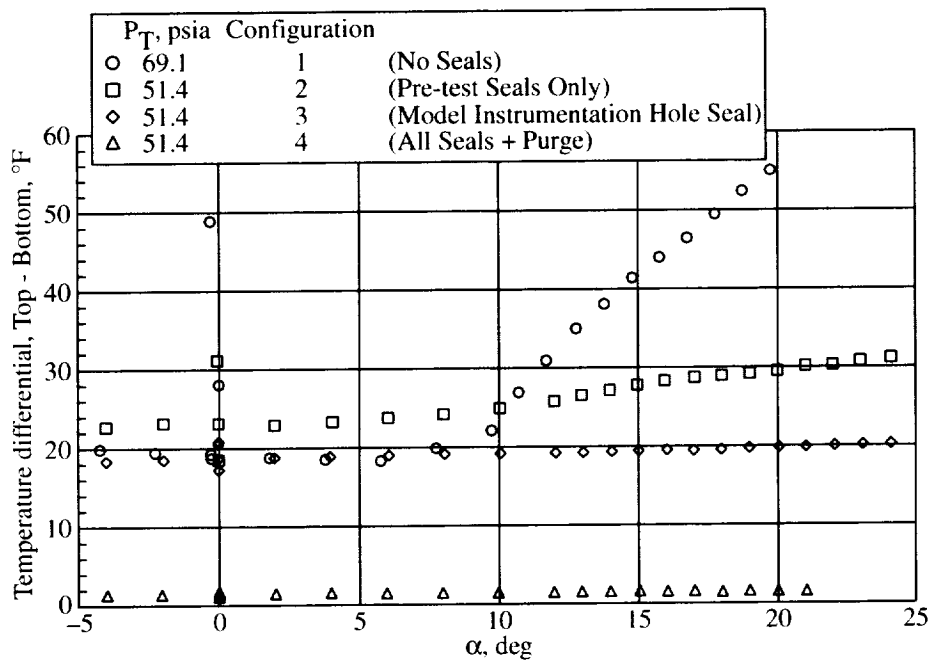


Figure 22. Effects of semi-span model support system improvements on balance temperature gradients.  $T_T = -250^\circ\text{F}$ .

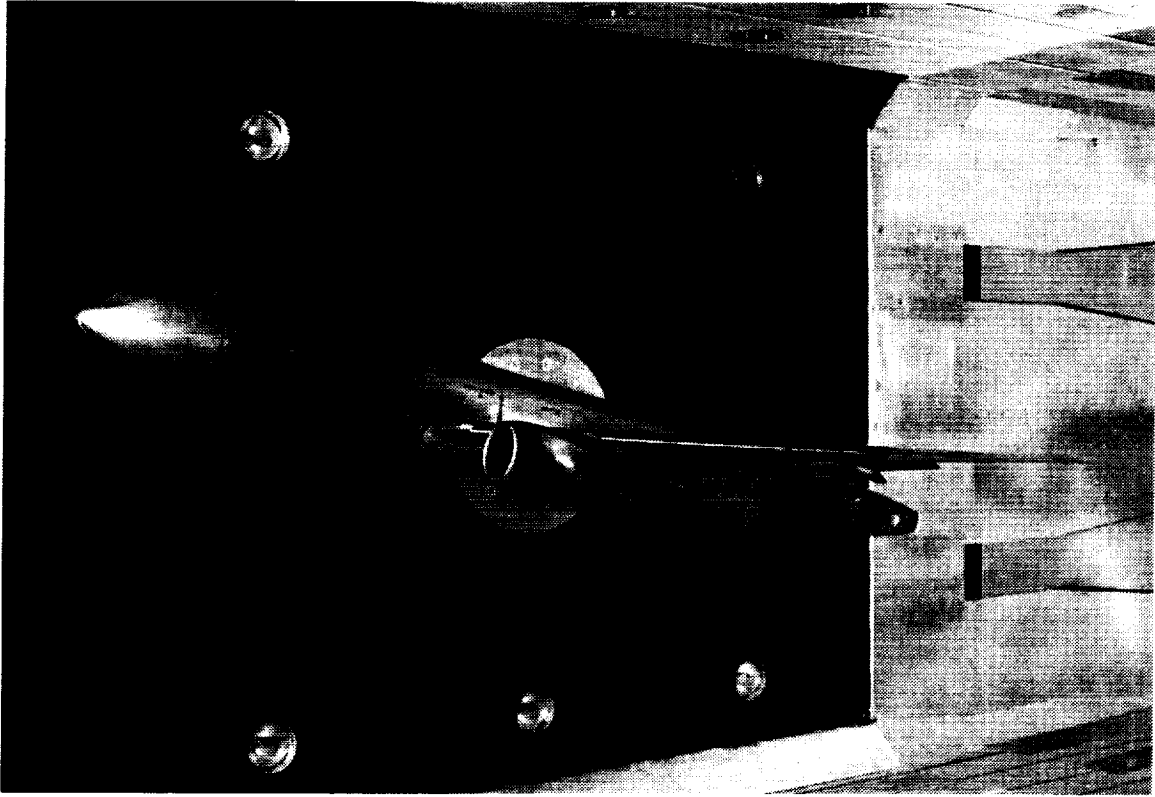


Figure 23. Photograph of takeoff configuration of 777 semi-span model in the NTF.

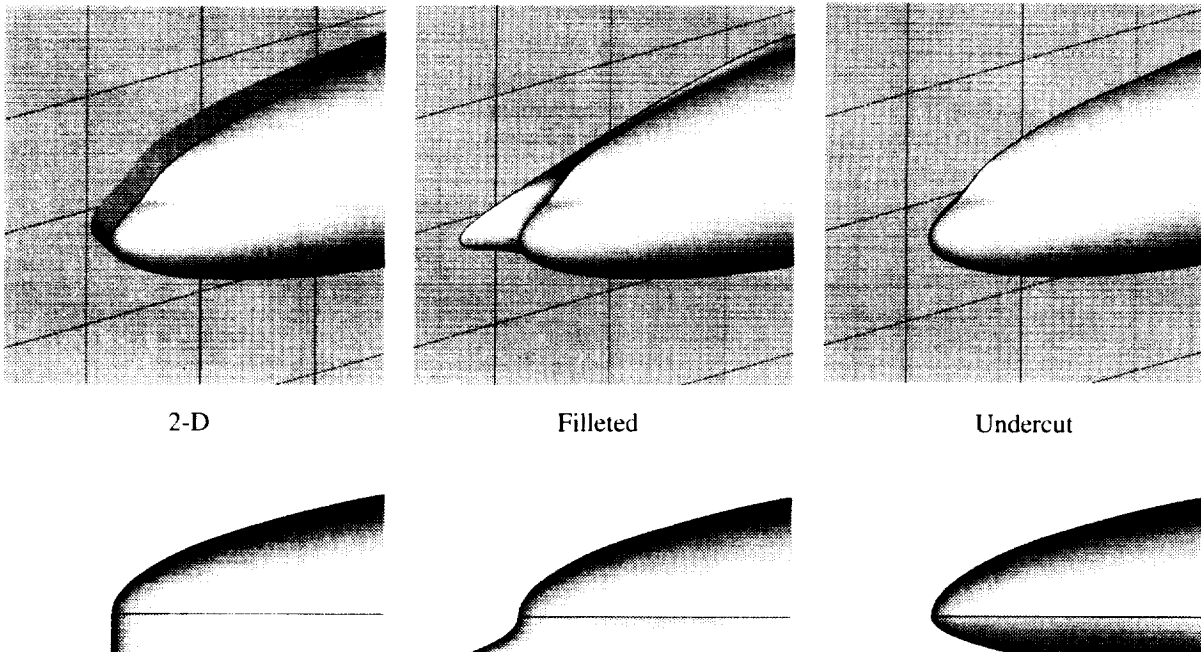


Figure 24. Standoff leading-edge shapes tested. [From reference 12.]

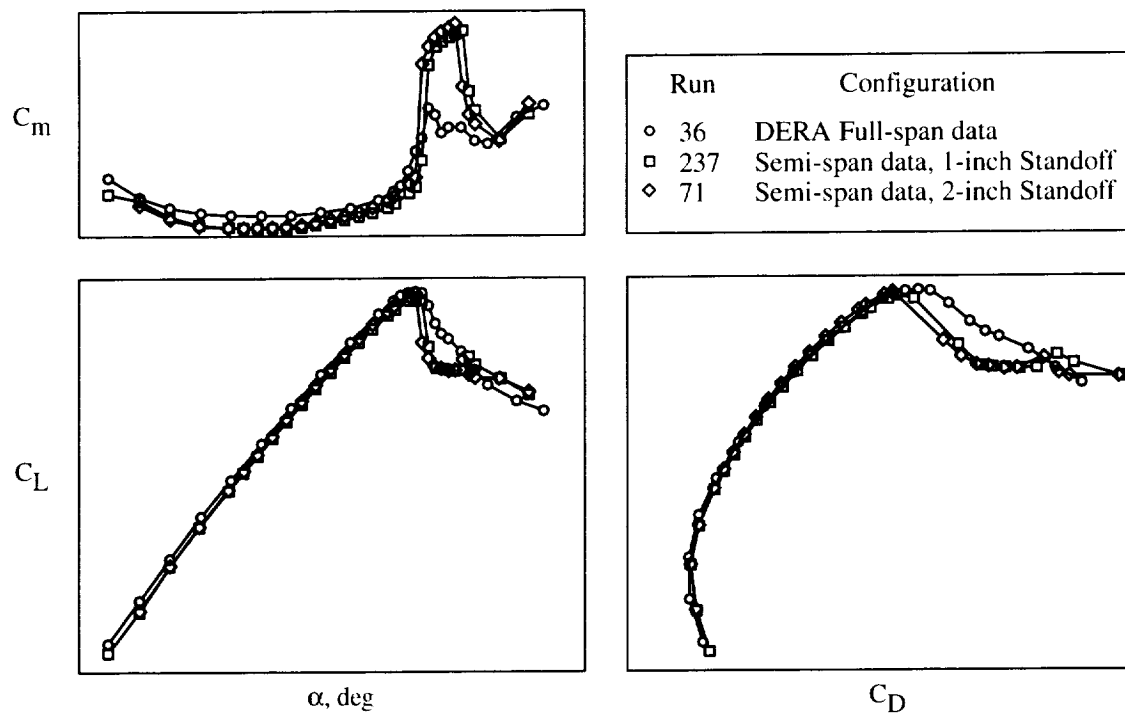


Figure 25. Effect of standoff height variation.  $M_\infty = 0.26$ ,  $R_c = 6.85 \times 10^6$ .

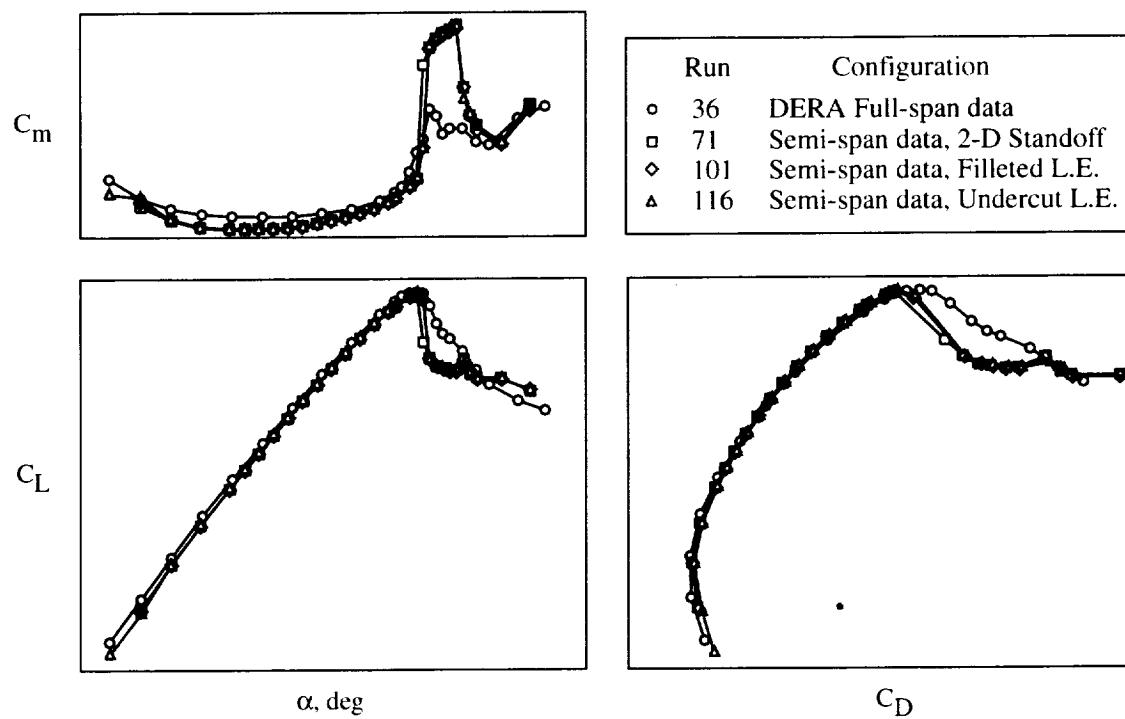


Figure 26. Effect of 2-inch standoff leading edge shape variation.  $M_\infty = 0.26$ ,  $R_c = 6.85 \times 10^6$ .

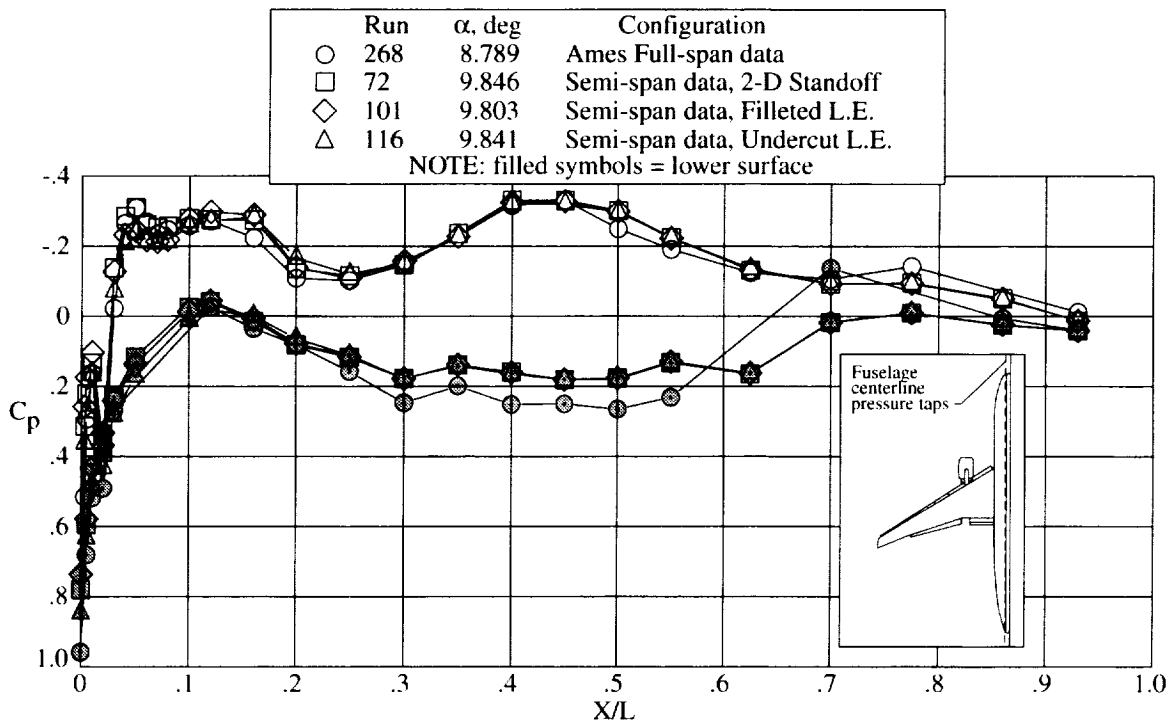


Figure 27. Fuselage centerline pressure data illustrating effects of 2-inch standoff leading edge shape variation.  $M_\infty = 0.26$ ,  $R_{\bar{c}} = 6.85 \times 10^6$ .

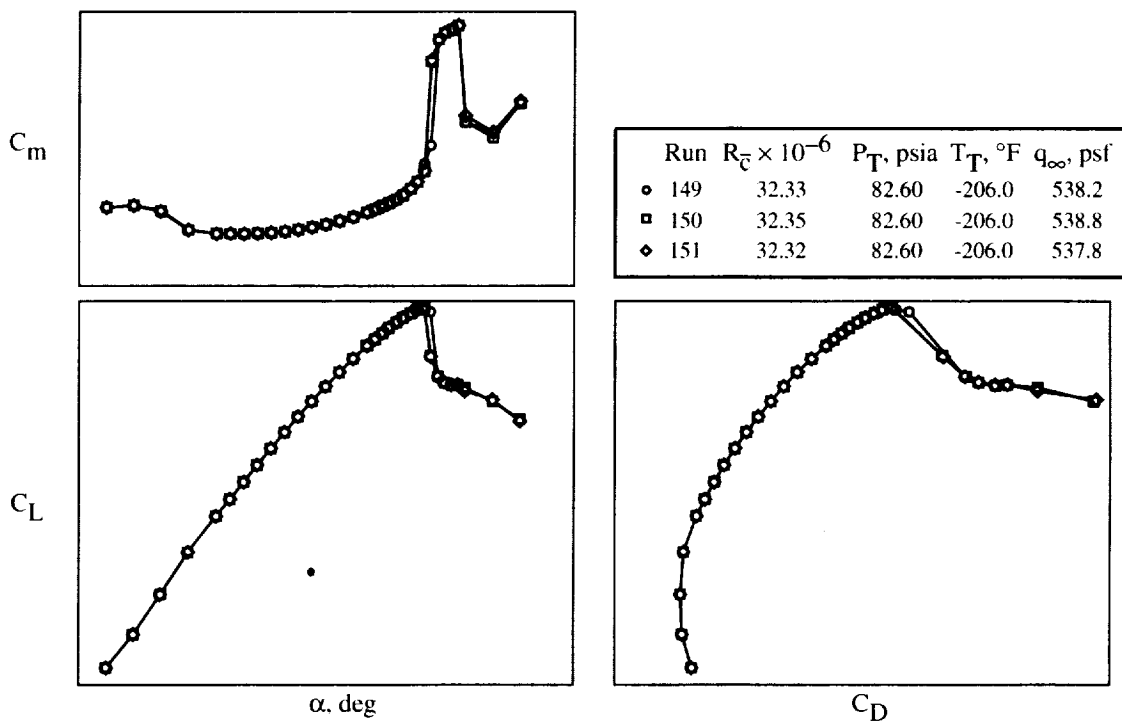


Figure 28. Data repeatability for nitrogen mode of operation at  $-206^\circ\text{F}$ .  $M_\infty = 0.26$ .

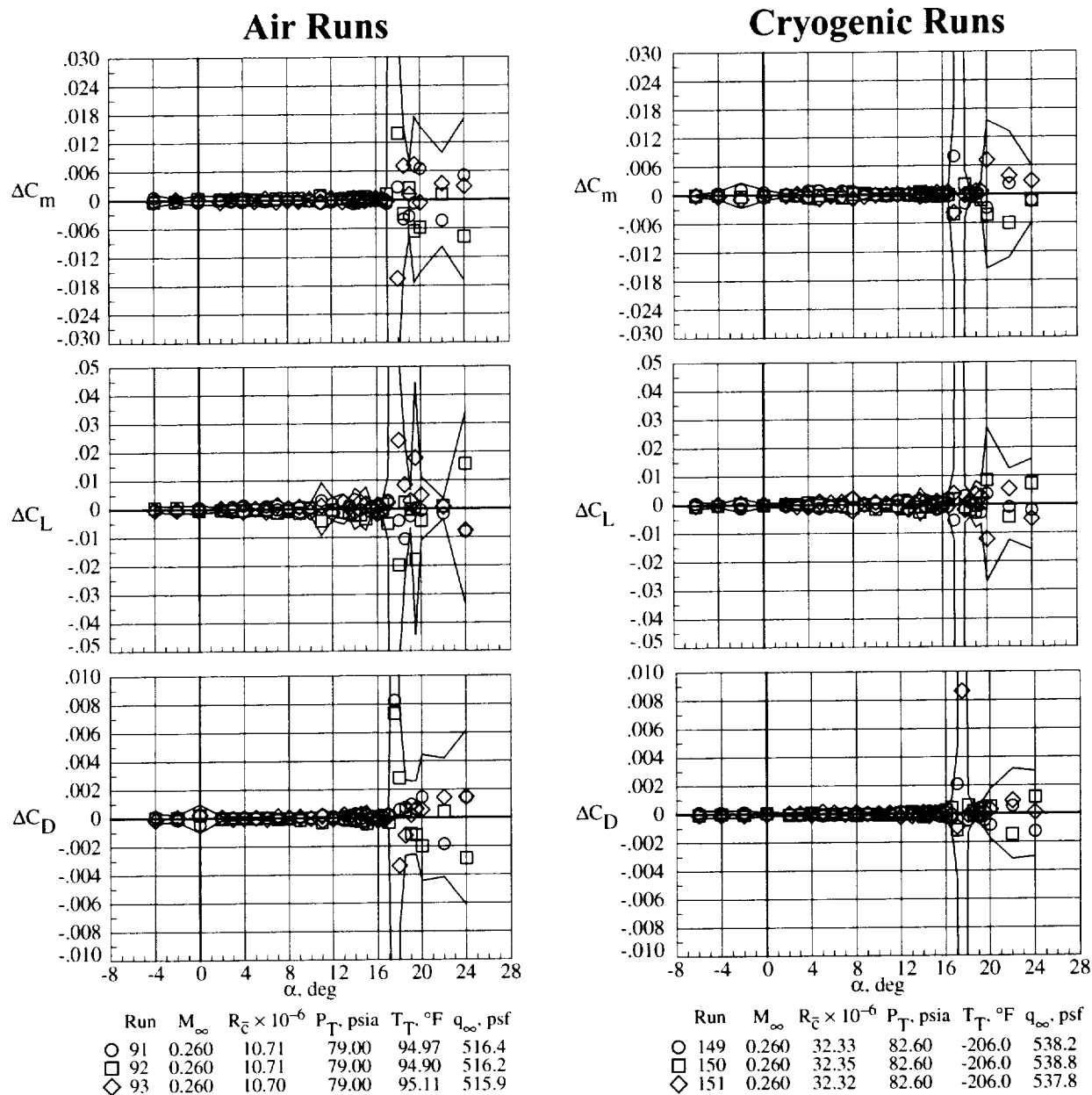


Figure 29. Comparison of air and cryogenic data repeatability.



/

